DINÇER YAKIŞIR

DEVELOPMENT OF GAS DIFFUSION LAYER FOR PROTON EXCHANGE MEMBRANE FUEL CELL, PEMFC

Mémoire présenté
à la Faculté des études supérieures de l'Université Laval
dans le cadre du programme de maîtrise en génie chimique
pour l'obtention du grade de maître ès sciences (M.Sc.)

FACULTÉ DES SCIENCES ET DE GÉNIE
UNIVERSITÉ LAVAL
QUÉBEC

2006

ABSTRACT

Presently, fuel cell technology is one of the most exciting fields in the area of new energy development with high scientific and technological challenges. Progress made up to now in the field of Proton Exchange Membrane Fuel Cell, PEMFC, technology offers large perspectives of applications. The interest in this environmentally benign technology has grown during the last years due to the Kyoto protocol requirements. However, a drastic decrease in PEMFC cost is needed prior to the widespread acceptance of PEMFC as automotive power systems.

The main objective of this study was to develop a new concept of high performance and low-cost porous electrode gas diffusion layer for PEMFC. Novel and industrially viable processing techniques based on twin-screw extrusion, post-extrusion film stretching or selective dissolution treatment were used. Conventional materials presently used for PEMFC electrodes were replaced in this project by new formulations based on highly filled thermoplastic polymers.

To create the porous structure of the gas diffusion layer, two different techniques were used. For the first technique, a thin film was made from low viscosity polypropylene, PP, filled with high specific surface area carbon black and synthetic flake graphite. Conductive blends were first prepared in a co-rotating twin-screw extruder and subsequently extruded through a sheet die to obtain films of around 500 microns in thickness. These films were then stretched in two successive steps to generate a film (100-200 microns) of controlled porous structure. However, for the second technique, the thin film was made from two immiscible polymers filled with a mixture of electronic conductive additives via twin-screw extrusion followed by selective extraction of one of the two polymers. The two polymers were a low viscosity PP and polystyrene, PS, and the conductive additives were the same as those used in the first technique. Conductive blends were first compounded in a co-rotating twin-screw extruder and subsequently extruded through a flexible film die to obtain a 500 microns film of high

electronic conductivity. The PS phase was then extracted with tetrahydrofuran, THF, solvent and a film of controlled porosity was generated. The morphology of the porous structures was then analyzed by scanning electron microscopy, SEM, and by BET surface area measurements. The effects of PS concentration and extraction time with THF on film conductivity and porosity were also studied.

RÉSUMÉ

Actuellement, la technologie des piles à combustible représente l'un des champs les plus passionnants avec des défis scientifiques et technologiques élevés. Les progrès réalisé jusqu'à date dans le domaine des piles à combustibles à membrane échangeuse de proton, PEMFC, offre de grandes perspectives d'applications. L'intérêt pour cette technologie non polluante a fortement grandit durant les dernières années à cause des conditions exigeantes du protocole de Kyoto. Cependant, l'optimisation des coûts de production des piles de type PEMFC est nécessaire avant leur intégration en tant que systèmes d'alimentation des véhicules à moteur.

L'objectif principal de cette étude était de mettre au point un nouveau design non coûteux de couche poreuse de diffusion de gaz pour électrodes de piles PEMFC. Des techniques pouvant être intégrées à l'échelle industrielle qui sont basées sur l'extrusion bi-vis, l'étirage post-extrusion de film mince ou la dissolution sélective ont été utilisés. Les matériaux conventionnels présentement utilises pour fabriquer les électrodes ont été remplacés dans le cadre de ce projet par des nouvelles formulations basées sur les polymères thermoplastiques fortement chargés avec des additifs à conductivité électronique élevée.

Pour créer la structure poreuse de la couche de diffusion de gaz, deux techniques différentes ont été employées. Pour la première technique, un film a été développé à partir d'une matrice en polypropylène, PP, de faible viscosité, chargé d'un grade spécial de noir de carbone possédant une surface spécifique élevée et de graphite synthétique en forme de feuillets. Les mélanges conducteurs ont d'abord été préparés dans une extrudeuse co-rotative bi-vis puis poussés à travers une filière plate. Cela a permis d'obtenir des films d'environ 500 microns d'épaisseur. Ces films ont ensuite été étirés en deux étapes successives afin de produire des films (de 100 à 200 microns) à structure poreuse contrôlée. En ce qui concerne la seconde technique, le film fin a été obtenu en mélangeant deux polymères immiscibles puis en y additionnant un mélange de charges électriquement conductrices. Cette opération a été menée en extrusion bi-vis. Elle a ensuite été suivie d'une extraction sélective de l'un des deux polymères. Les deux polymères dont il s'agit sont le PP à basse viscosité et le polystyrène, PS.

Les charges conductrices sont les mêmes que celles utilisées à la première technique. Ces mélanges conducteurs ont été composés dans une extrudeuse co-rotative bi-vis puis poussés à travers une filière plate flexible afin d'obtenir un film de 500 microns à grande conductivité électrique. Le phase PS a été extraite par la suite grâce à un solvant : le tétrahydrofurane, THF. Des films à porosité contrôlée ont ainsi été générés. Les morphologies des structures poreuses ont été analysées par microscopie électronique à balayage, SEM, ainsi que par des mesures de surfaces spécifiques BET. Les effets de la concentration du PS et du temps d'extraction sélective par THF sur la conductivité et la porosité des films ont également été étudiés.

ACKNOWLEDGEMENTS

First, I would like to express my sincere gratitude to my supervisor, Professor Frej Mighri, for his guidance, help and encouragement throughout the course of this project and also for giving me the possibility to work on this research subject. It has been a great opportunity for me to be able to make a dissertation under his supervision on such interesting subject.

I would also like to thank my research co-supervisor, Professor Mosto Bousmina, for all his helpful comments and advices throughout my studies.

Special thanks go to my colleagues for all their help and advices along this master program. In particular, I would like to thank Marlaine Rousseau and Steve Pouliot for their assistance during the laboratory work. Also, I would like to thank all my friends at the department of chemical engineering for their friendship and helps. Especially, I thank Bora Aydin for all his helpful guidance and moral support over the last few years.

Finally, I would like to express my deepest thanks to my mother, Hacer, and to my father, Enver, for their never-ending support and encouragement throughout my studies. This is for you.

TABLE OF CONTENTS

LIST OF TABLES

LIST OF FIGURES

CHAPTER 1

Introduction

Industrial era started with the discovery of steam engine in 1765. From that time until today, the consumption of fossil fuels has been increasing enormously. For example, the global energy consumption has increased over 14% during the last decade. Today, it is known that the increasing levels of greenhouse emissions are changing the earth's climate. Hence, new power sources, environmentally friendlier and more efficient than the conventional ones, must emerge. One of the most promising candidates, may be the best to overcome the pollution problems, is fuel cell technology. Therefore, during the last few decades, a tremendous effort in research and development was undertaken to improve and commercialize this clean energy source.

Fuel cells are electrochemical devices that convert chemical energy directly into electrical energy and heat, similar to batteries. However, unlike a battery, the reactants in a fuel cell are stored externally and therefore they produce energy continuously as long as the reactants are supplied. Internal combustion engines convert thermal energy into mechanical energy which is limited by Carnot's law. Unlike internal combustion engines, fuel cells provide zero or near

zero emissions, which makes them as an attractive option for a wide range of applications, such as transportation, stationary power generation, and portable application.

Depending on the electrolyte employed, various types of fuel cells currently exist in the market. The main types are: Alkaline fuel cells (AFC), Molten carbonate fuel cells (MCFC), Phosphoric acid fuel cells (PAFC), Solid oxide fuel cell (SOFC), and Proton Exchange Membrane Fuel Cells (PEMFC).

1.1 HISTORY

The history of fuel cell had begun with the experimental work of the British judge and amateur scientist, Sir William Robert Grove who developed, in 1839, a system in which hydrogen and oxygen were mixed in the presence of an electrolyte in order to produce electricity. To improve the voltage, he connected several individual systems in series [1]. However, his developed system, that was called fuel cell later, was not able to produce enough electricity to be useful.

The expression "fuel cell" was firstly used by the chemists Ludwing Mond and Charles Langer in 1889, who tried to construct a working fuel cell by using air and industrial coal gas. By the end of 20th century, the fuel cell becomes less important for the scientific research due to the invention of the internal combustion engine, which made the consumption of fossils fuels more popular.

Dr. Francis Thomas Bacon did the next scientific attempt in 1932. He developed an apparatus, called "Bacon cell", which is known as the first alkaline fuel cell (AFC). Indeed, this apparatus was a modified version of the fuel cell developed by Ludwing Mond and Charles Langer. However, it took around 27 years for Bacon to develop a 5 kW prototype.

The major discovery in fuel cell history was done by National Aeronautics and Space Administration, NASA, researchers in 1950th, who developed the first Proton Exchange Membrane fuel cell, PEMFC, prototype. In 1955, Willard Thomas Grubb modified this

prototype by using a sulphonated polystyrene ion-exchange membrane as the electrolyte and, three years later, Leonard Niedrach developed a technique to adequately deposit the platinum on to the membrane. The modified design was known as "Grubb-Niedrach fuel cell". General Electric and NASA used the first commercial fuel cell in the "Gemini Space Project" to provide on-board electricity and water to the Gemini, Apollo and space shuttle mission [1, 2].

In 1993, the first fuel cell-powered vehicle was developed by Ballard, a Canadian company. Recently, practical applications of fuel cells can be seen in daily life such as in hospitals, schools, and some transportation vehicles. Presently, most of the automobile companies produce their own prototype fuel cell powered cars.

1.3 DIFFERENT TYPES OF FUEL CELLS

The basic structure of a fuel cell, their corresponding reactants and product gases are sketched in Figure 1-1.
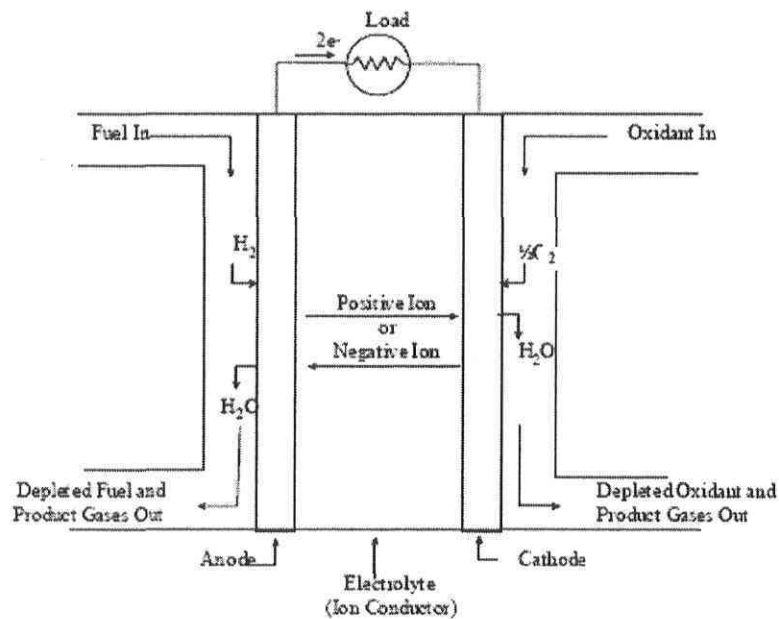
Figure 1-1 Structure of a fuel cell [3].

Reactants are fed continuously to the fuel cell electrodes separately. Gaseous fuels (generally hydrogen) are fed to the anode where chemical reaction strips them of their electrons. Oxidants (oxygen from air) are fed to the cathode. All the electrochemical reactions occur at the electrodes for generating electric current. Theoretically, fuel cells are able to produce electrical energy as long as the reactants are supplied to the electrodes. However, operating life is practically limited because of the malfunction, corrosion and degradation [1].

According to Appleby and Foulkes [4], any material that has an ability of chemical oxidation can be used continuously as a fuel at the anode side of the fuel cell. Hydrogen is generally used because of its good reactivity with suitable catalysts. Like hydrogen, oxygen is the most used oxidant. It is economically available from air and can be easily stored in closed environment.

There are several types of fuel cells and their operating principles are generally the same. They are usually categorized by their type of electrolyte (membrane), which dictates the optimal operating temperature and the kind of reactants to be used. The main types of fuel cells are briefly presented in the following sections. However, more details are given in Section 1.4 for proton exchange membrane fuel cell, PEMFC.

1.3.1 Alkaline Fuel Cells (AFC)

Alkaline fuel cells are operated under compressed hydrogen and oxygen. An aqueous solution of potassium hydroxide (KOH) is used as the electrolyte and a wide range of precious metals (e.g. Ni, Ag, metal oxides, and noble metals) as electro-catalysts. In electrolyte, different percentages of KOH are used for different operating temperatures ranging from $65^{\circ}C$ to $220^{\circ}C$.

Presently, most of AFC are operated at low temperatures ($<80^{\circ}$) and are known as high performance fuel cells due to their good chemical reaction rate. AFC are very sensitive to carbon dioxide (CO_2) that may be present in the fuel or air. CO_2 in any reformed fuel reacts with potassium hydroxide (KOH) electrolyte to form a solid carbonate, which destroys the

electrolyte ion mobility. So, a small amount of CO_2 degrades the fuel cell performance. Hence, it is important to purify both the hydrogen and oxygen. However, purification of hydrogen and oxygen is expensive and their use was restricted to some special applications only, such as space and undersea vehicles.

The electrochemical AFC reactions at the cathode and anode sides are shown below.

Anode: $$H_2 + 2OH^- \rightarrow 2H_2O + 2e^- \tag{1-1}$$

Cathode: $$O_2 + 2H_2O + 4e^- \rightarrow 4OH^- \tag{1-2}$$
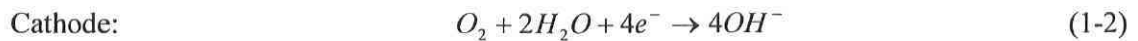
Hydroxyl ions are the conducting species in the electrolyte and the net fuel cell reaction is:

$$2H_2 + O_2 \rightarrow 2H_2O + electric.energy + heat \tag{1-3}$$

1.3.2 Molten Carbonate Fuel Cells (MCFC)

The electrolyte of MCFC concentrated high temperature compounds of molten carbonate salts suspended in a porous and chemically inert ceramic lithium aluminum oxide (L_iAlO_2) matrix. MCFC operate at high temperatures (around 650^oC or above). High operating temperature is needed in order to melt the carbonate salts and to ensure high ion mobility through the electrolyte. Molten salts become conductive to carbonate ions $(CO_3)^{2-}$. Carbonate ions flow from cathode to the anode where they combine with hydrogen to give water, carbon dioxide and electrons.

The electrochemical reaction equations of the half-cells and the overall cell reaction are the following:

Anode: $$H_2 + CO_3^{-2} \rightarrow H_2O + CO_2 + 2e^- \tag{1-4}$$

Cathode: $$1/2O_2 + CO_2 + 2e^- \rightarrow CO_3^{-2} \tag{1-5}$$

The overall cell reaction: $$H_2 + \frac{1}{2}O_2 + CO_2 \rightarrow H_2O + CO_2 \tag{1-6}$$
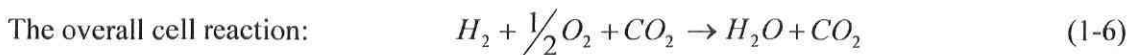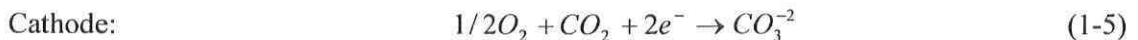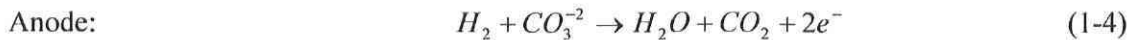
High operating conditions allow the use of lowest non-precious metals as catalyst either in the anodes or in the cathode sides. At high temperatures, fuels are also converted to hydrogen within the fuel cell (internal reforming). Hence, MCFC don't need any external reformer to

convert the fuel into hydrogen unlike the other type of fuel cells. Furthermore, they have higher resistance to impurities. However, the high temperature needed for MCFC operation requires significant time to reach the operating conditions. The high operating temperature and corrosive electrolyte also limits the materials and safe uses of MCFC [3]. These characteristics make them more suitable for constant power applications like in hospitals, hotels, etc.

1.3.3 Phosphoric Acid Fuel Cells (PAFC)

PAFC are considered as the "first generation" of modern fuel cells. Presently, PAFC are worldwide commercialized [3]. The electrolyte consists of liquid phosphoric acid, which is contained in a Teflon-bonded silicon carbide matrix. The electrode of PAFC contains platinum catalyst, like in proton exchange membrane fuel cells. PAFC are generally used for stationary power generation. However, some PAFC have been used in large vehicle, like in city buses.

At low temperatures, phosphoric acid is a poor ionic conductor. Consequently, PAFC are operated between $150^{\circ}C$ and $200^{\circ}C$. High acid concentration increases PAFC performance. The PAFC operates at more than 40 percent of efficiency in generating electricity. However, when they are used for the co-generation of electricity and heat, the overall efficiency can reach approximately 85 percent.

The electrochemical reactions that occur at both electrodes are as follows:

Anode: $$H_2 \rightarrow 2H^+ + 2e^- \qquad (1\text{-}7)$$

Cathode: $$2H^+ + \tfrac{1}{2}O_2 + 2e^- \rightarrow H_2O \qquad (1\text{-}8)$$

Overall: $$H_2 + \tfrac{1}{2}O_2 \rightarrow H_2O \qquad (1\text{-}9)$$
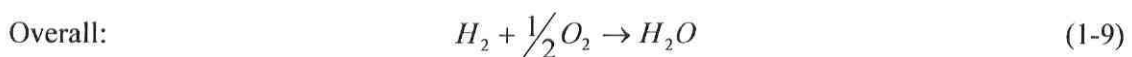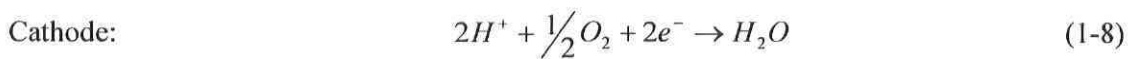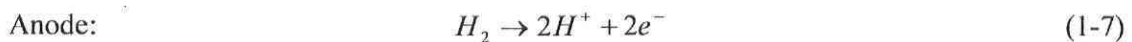
1.3.4 Solid Oxide Fuel Cells (SOFC)

The electrolyte of SOFC is fabricated from the non-porous ceramic compound of calcium or zirconium. The operating efficiency in generating electricity is around 50-60 percent.

However, when the co-generation system is used for the waste heat, the overall efficiency may increase to around 80-85 percent.

SOFC are the best systems in resisting to sulphur. They can tolerate more sulphur than the other fuel cell types. Furthermore, they don't poison by carbon monoxide (CO) and therefore, CO can be used as a fuel like in MOFC.

High operating temperatures (> 800°C) allows internal reforming, rapid kinetic with non-precious materials. SOFC require significant time to reach the operating temperature and their response to the electricity demand is slow. Furthermore, a thermal shielding should be used to ensure safe operation environment. Therefore, SOFC are best suited for large-scale stationary power applications containing industrial and large-scale central electricity generating stations.

High operating temperature increases the deterioration rate of fuel cell components. Therefore, the main technical challenge facing SOFC is to develop a low-cost material with high durability.

The electrochemical reactions in SOFC are:

Anode: $$H_2 + O^{-2} \rightarrow H_2O + 2e^-$$ (1-10)

Cathode: $$\frac{1}{2}O_2 + 2e^- \rightarrow O^{-2}$$ (1-11)

Overall: $$H_2 + \frac{1}{2}O_2 \rightarrow H_2O$$ (1-12)
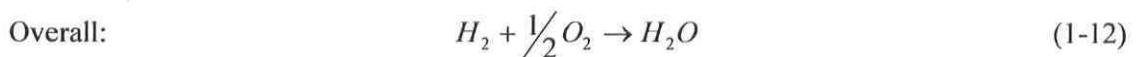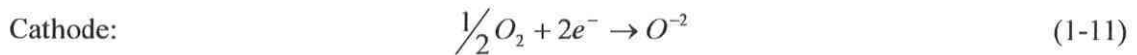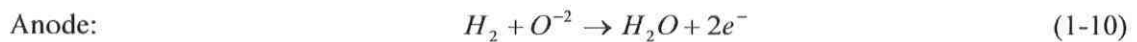
1.3.5 Comparison of Fuel Cell Technologies

As mentioned in Section 1.1, fuel cells are generally classified according to their electrolyte. The electrolyte defines the key parameters, particularly the optimal operating temperature of the fuel cell. The main features of the five major fuel cell technologies are summarized in Table 1-1.

Table 1-1 Comparison of the five major fuel cell types.

TYPE OF FUEL CELL	PROTON EXCHANGE MEMBRANE (PEM)	PHOSPHORIC ACID (PAFC)	MOLTEN CARBONATE (MCFC)	SOLID OXIDE (SOFC)	ALKALINE (AFC)
Electrolyte	Ion Exchange Membrane	Liquid Phosphoric acid	Molten Carbonate Salt	Solid Metal Oxide	Potassium Hydroxide
Efficiency Without Cogeneration With Cogeneration	35-50% 60%	35-50% 80%	45-60% 85%	45-60% 85%	40-60%
Operating temperature	60-100°C	150-200°C	600-1000°C	600-1000°C	80-250°C
Power output	0.1kW – 250kW	200kW – 1MW	1MW – 200MW	2kW – 2MW	0.1kW – 20kW
Catalyst	Platinum	Platinum	Nickel	Perovskites	Platinum
Oxidant	O_2/Air	O_2/Air	CO_2/O_2/Air	O_2/Air	O_2/Air
Reforming	External	External	External/Internal	External/Internal	-
Limitation	Manufacturing Cost, Need pure hydrogen, no tolerance for contaminates; complex heat and water management.	Low efficiency Limited service life Expensive catalyst	Electrolyte instability Limited service life	High operating temperature; requires exotic metals, high manufacturing cost, oxidation issues; low specific power.	Large size; needs pure hydrogen and oxygen, Usage of corrosive liquid electrolyte.
Advantages	Compact design; relatively long operating life, adapted by major automakers, quick start-up, low temperature operation	Commercially available, lenient to fuels, utilizes heat for co-generation.	Highly efficient, use heat to run turbines for co-generation.	High efficiency, lenient to fuels, takes natural gas directly, no reformer needed. Uses heat for co-generation.	Low manufacturing and operating costs. Does not need heavy compressor, fast cathode kinetics.
Applications	Transportation, portable power, electric utility	Electric utility, transportation	Electric utility	Electric utility	Military Space

1.4 POLYMER ELECTROLYTE MEMBRANE FUEL CELL, PEMFC

The first PEMFC was built up in the 1960s as an auxiliary power source in the Gemini space flights [5]. In 1960s, a perfluornated sulfonic acid ionomer membrane, invented by Dupont under the commercial name Nafion®, helped to reduce the PEMFC cost without decreasing its efficiency. At the end of 1980s, low platinum loaded electrodes were developed [6, 7] and lead to cheaper PEMFC for the commercial markets. In the last few decades, rapid development in PEMFC technology made them adequate to be used in commercial scale, especially for transportation. Presently, several automotive companies have already been produced prototypes of fuel cell electrical vehicles.

The schematic structure of a PEMFC, together with an illustration of the operating principle, is given in Figure 1-2. The PEM fuel cell uses hydrogen gas as the fuel and oxygen (generally from air) as the oxidant. Hydrogen molecules split on the anode into protons and electrons. The protons are conducted through the proton exchange membrane. The electrons, which cannot cross the membrane (an electronic insulator), are conducted to the cathode through the external circuit to produce electricity. On the cathode side, oxygen, protons and electrons combine to form water.

The electrochemical reaction for PEM fuel cell is:

Anode Side: $\qquad H_2 \rightarrow 2H^+ + 2e^-$ $\qquad\qquad$ (1-13)

Cathode Side: $\qquad \dfrac{1}{2}O_2 + 2H^+ + 2e^- \rightarrow H_2O$ $\qquad\qquad$ (1-14)

Total cell reaction: $\qquad H_2 + \dfrac{1}{2}O_2 \rightarrow H_2O + electricity + heat$ $\qquad\qquad$ (1-15)
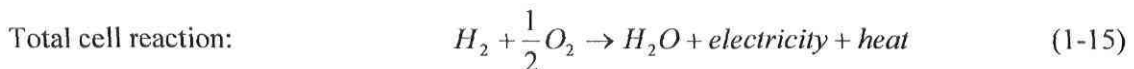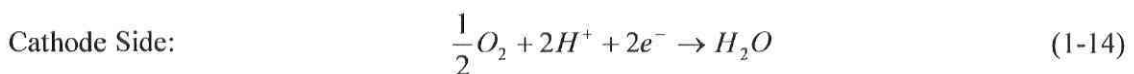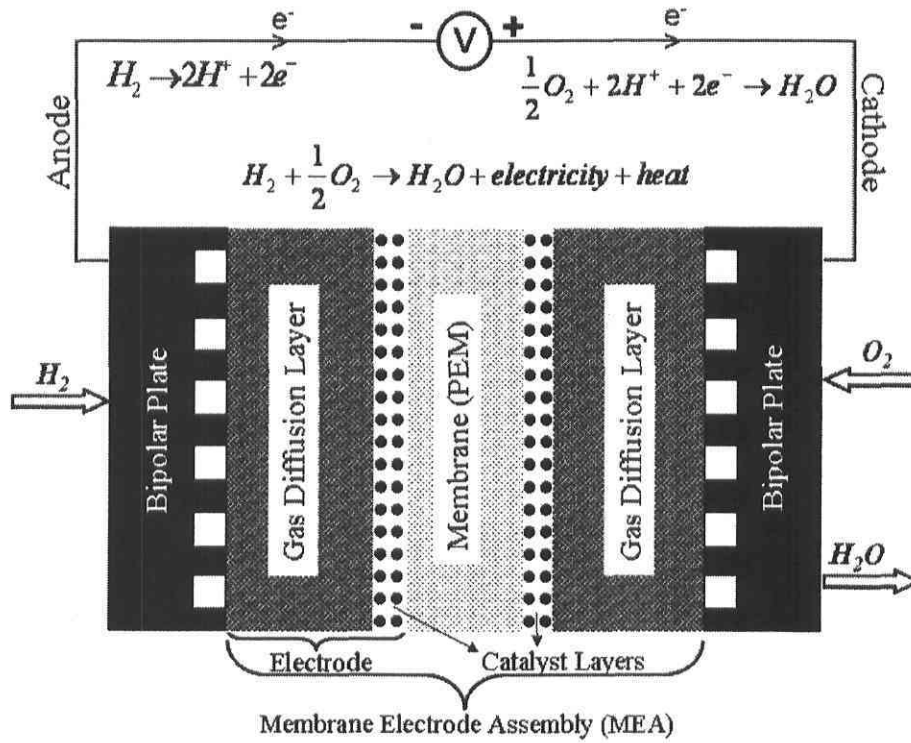
Figure 1-2 Structure of a PEM fuel cell, showing the electrochemical reactions.

Actually, the half reactions in the electrodes occur very slowly. This slow reaction reduces the efficiency of the PEMFC. Therefore, to increase the speed of reaction, catalysts are used. All the reactions occur on catalyst surface. Platinum is the best known catalyst because it is sufficiently reactive in bonding H and O intermediates:

$$H_2 + 2Pt \rightarrow 2Pt - H$$
$$2Pt - H \rightarrow 2Pt + 2H^+ + 2e^-$$

(1-16)
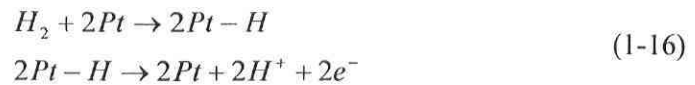
The membrane electrode assembly (MEA) is the heart of the PEMFC. It is typically sandwiched between two electronically conductive bipolar plates and it is composed of layered structures consisting of two electrodes and one proton exchange membrane, PEM. The various layers are fabricated individually and then pressed together at the high temperature to form a unique multilayer structure.

1.4.1 Proton Exchange Membrane (PEM)

The electrolyte of a PEMFC is a protonic conductive membrane made from polymers. This membrane provides a proton conductive zone to allow the protons to pass from the anode to the cathode side. It must be a good electronic insulator in order to force the electrons to use external circuit for generating electricity. The organic nature of the polymer electrolyte membrane structure makes them electronic insulators. In addition, the membrane has to be impermeable to reactant gases in order to prevent the direct oxidation of the fuel. It should also be mechanically and chemically stable.

Currently, the most common material used as PEM is Nafion®, a trademark of Dupont. The structure of Nafion is shown in Figure 1-3. It consists of a polytetrafluoroethylene backbone on which sulfonic acid groups are bonded. The Nafion membrane exhibits exceptionally high chemical and thermal stability. However, it must remain hydrated in order to ensure proton conductivity. This limits the operating temperature of PEMFC under the boiling point of water (i.e., less than 100°C). Consequently, water management is another key issue in PEMFC development. Some alternative polymer electrolyte materials, more effective and more economical, are currently under development [1, 9, 10].

$$-[(CF_2-CF_2)_x-(CF_2-CF)]_y-$$
$$|$$
$$O-CF_2-CF-CF_3$$
$$|$$
$$O-CF_2-CF_2-SO_3H$$
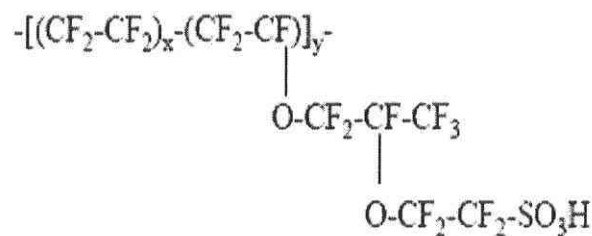
Figure 1-3 Structure of Nafion®.

1.4.2 PEMFC Bipolar Plates

Other important parts of the PEMFC stack are the bipolar plates, which are situated next to the gas diffusion layer. The main functions of the bipolar plates are to distribute the fuel and

11

oxidant within the cell and to help the water management within the cell by removing residual water. Bipolar plate materials should have high electronic conductivity in order to carry current between adjacent cells and must be impermeable to the reacting gases and ions. Furthermore, bipolar plates have to be chemically inert to the reactant gases and products, and should remove the heat from the active area of cell. In addition, for most PEMFC applications, especially for automotive industry, lightweight and high strength are ones of the other most requirements [11, 12].

Bipolar plates are usually made from graphite because of its good electrical and heat conduction properties, its mechanical rigidity, and its chemical stability. There are also some other promising materials for fabricating bipolar plates, such as stainless steel, coated metals and polymer-carbon composites [13]. For commercial application, bipolar plate materials should not be expensive and must have suitable processing properties for high-volume manufacturing.

One major drawback of graphite is the high cost of the bulk material. Also, it is difficult to machine gas distribution and cooling channels on graphite. PEMFC bipolar plates made from graphite are also relatively heavy. They represent about 80% of the total weight of the cell stack.

Like graphite, stainless steel has good features. However, they are expensive to machine and need to be coated to avoid corrosion and to reduce the contact resistance. For commercial market, the best results have been achieved with carbon-polymer composites, which can be easily fabricated by injection or compression molding processes [11, 14].

The flow channel geometry on bipolar plates has also considerable effects on PEMFC performances, such as on reactant flow velocities and on mass transfer. These channels are used to carry the reactant gases from the point at which it enters the fuel cell to the point at which the gas exists. There are several criteria that must be taken into account in bipolar plate channel geometry optimization, which is not the scope of this project.

1.4.3 PEMFC Electrodes

A typical PEMFC electrode, generally less than 400µm in thickness, consists of two porous thin layers: the backing or gas diffusion layer and the active catalyst layer. All chemical reactions occur in the electrode: The oxidation half-reaction at the anode side and the reduction half reaction at cathode side. However, it should be mentioned that these two half reactions occur very slowly at low PEMFC operating temperatures (around 80°C). Consequently, catalysts, such as platinum, Pt, are used on both electrodes, at the anode and cathode sides, in order to increase the rates of these half reactions.

For an effective operation of a PEMFC, electrode constituting materials should be correctly balanced (see Figure 1-4). A good electrode must provide i) proton conductivity at the membrane/electrode interface, ii) electrons conductivity from the catalyst layer to the bipolar plates via the gas diffusion layer, and iii) the transport of the reactant and product gases to and from the catalyst layer.
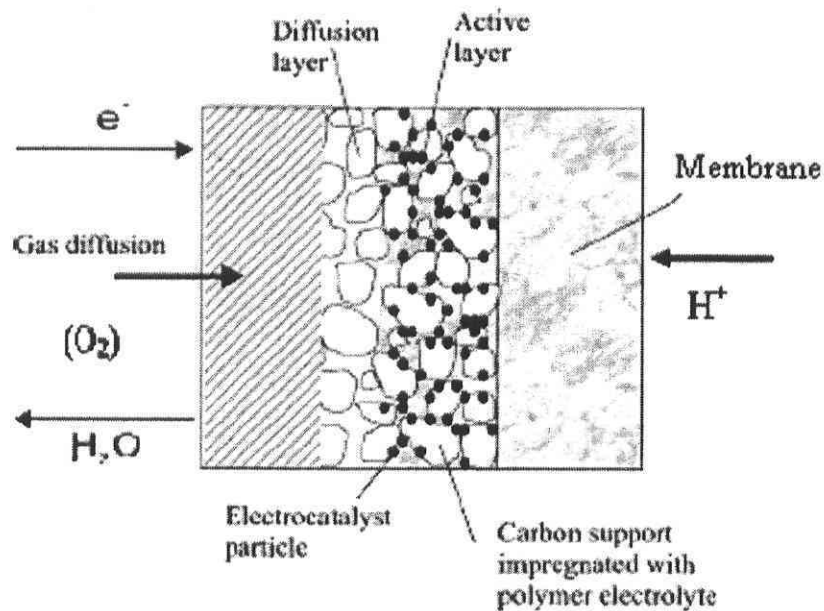
Figure 1-4 Transport process in PEMFC electrode [15].

1.4.3.1 PEMFC Catalyst Layer

The catalyst layer (of thickness less than 100 μm), also known as active or reactive layer, is in direct contact with the proton exchange membrane and the gas diffusion layer, at both cathode and anode sides. It is usually fabricated from platinum, Pt, catalyst supported on high surface area carbon black particles held together with binding agents, such as polytetrafluoroethylene (PTFE) or Nafion. The nature of PTFE also prevents flooding of the pores within the electrode. Carbon blacks are good electronic conductors and their porous structures ensure the pathway for reactants to the catalyst particles. Although PEMFC shows exceptional long term performances with these materials, their cost remains high for commercialization due to utilization of high amount of Pt. The main challenge in PEMFC technology is to reduce the amount of platinum usage in the catalyst layer. In some references [16, 17], it has been reported that the Pt loading amount can be reduced below 0.4 mg/cm^2. Further reduction in Pt loading (0.014 mg/cm^2 Pt loading) was achieved by using novel sputtering methods [18, 19]. After the invention of low loading Pt, the cost of catalyst does not represent any further obstacle for PEM fuel cell commercialization.

Wilson et al. [20] developed a catalyst layer by mixing the catalyst (20wt% Pt on carbon) with 5wt% of solubilized Nafion. The protonated form of Nafion within the ink is converted to the tetrabutylammonium (TBA$^+$) form by the addition of 1M TBAOH in methanol [21]. The mixture was cast onto membrane either "decal" process (in which the ink is cast onto Teflon blanks and transfer to the membrane by hot-pressing) or directly. Membrane-electrode assembly was completed by applying the gas diffusion layer on both sides of the catalyzed membrane. High performance with low catalyst loading (0.12mg Pt cm^{-2}) at the cathode and even lower loading at the anode was reported. The use of thermoplastic ionomer improved the reproducibility and long-term performance of fuel cell stacks.

Reactant diffusivity is also an important parameter for the catalyst layer. They should have a porous structure to ensure reactant diffusivity. Yoon et al. [22] investigated the effect of pore

structure of the catalyst layer in a PEMFC on its performance. The catalyst layer was fabricated by spray-drying method under various conditions, while Pt loading of 0.4 mg/cm^2 was kept constant at both anode and cathode sides. The effect of pore forming agents on the cell performance was also studied. They found that pore structure has an important effect on PEMFC performance. The addition of pore forming agents doesn't enhance the PEMFC performance. It only helps the oxygen transportation through the catalyst layer.

In addition to catalyst loading and reactant diffusivity, the hydrophobicity and protonic conductivity are also significant parameters for the catalyst layer. To ensure hydrophobicity and protonic conductivity, Nafion ionomer and PTFE binder have been used. Nafion ionomer is a good proton conductor. It transports the hydrogen proton across membrane to the catalyst surface for the electrochemical reaction. Nafion ionomer also helps moisture retention and prevents membrane dehydration. It is necessary to find the optimum Nafion content in catalyst layer for ensuring a good performance. Low loading of Nafion in the catalyst layer leads to a poor contact between the membrane and catalyst layer and consequently to a significant decrease in PEMFC performance. On the other hand, high loading of Nafion in the catalyst layer destroys the electrode performance because it obstructs the electrode pores.

Several studies have been done to investigate the optimum Nafion content in the catalyst layer. Paganin et al. [23] reported that cell performance increases when the Nafion loading is increased from 0.87 to 1.75 mg/cm^2. However, when the Nafion loading is increased beyond 2.2 mg/cm^2, which corresponds to 33wt% of catalyst layer, PEMFC performance decreases. This result has also been reported in the literature [24-26]. As shown in Figure 1-5, Qi and Kaufman [27] reported an optimum Nafion content in the catalyst layer of around 30wt%.

Sasikumar et al. [28] showed that optimum Nafion content in the catalyst layer increases with decreasing the Pt loading. For Pt loadings of 0.5, 0.25 and 0.1 mg/cm^2, the best performance was obtained with Nafion loading of 20, 40 and 50wt%, respectively.
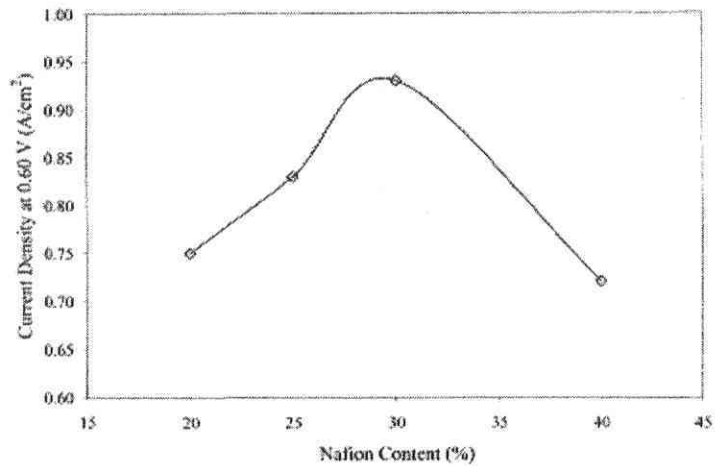
Figure 1-5 Effect of Nafion content in catalyst layer on the performance of PEMFC [27].

1.4.3.2 PEMFC Gas Diffusion Layer

Gas diffusion layer, GDL, which is located between the catalyst layer and bipolar plates, is the second part of the PEMFC electrode. It is usually fabricated from a porous carbon paper or carbon cloth, with a thickness of 100-300μ. The GDL porous structure ensures effective diffusion of each reactant from the flow channels to the catalyst layer. At the same time, the GDL must be able to transport electrons from the anode catalyst layer to the external circuit and from the external circuit to the cathode catalyst layer. Furthermore, they should assist water management inside the PEMFC. Therefore, GDL are generally wet-proofed with PTFE suspension to prevent flooding of the pores with water. However, the amount of PTFE should be carefully balanced because a high loading of PTFE could obstruct the pores [29]. Paganin et al. [23] developed a Teflon based GDL and found ant optimal PTFE content of around 15 wt%. The performance of the developed GDL increased with increasing its thickness from 15 to 35μm. Lee et al. [30] examined the effect of compression of different GDL on PEMFC performance. According to their experimental results, the type of GDL and the bolts (which hold the fuel cell stack together) have a significant effect on PEMFC performance. Lim et al. [31] studied the effect of hydrophobic polymer content in GDL on PEMFC performance. They prepared the GDL by treating commercial carbon papers with fluorinated ethylene propylene (FEP). Electrodes with 10wt% FEP-impregnated GDL provided the best performance. Further

increase in FEP content lead to a decrease in the performance of PEMFC and excessive FEP impregnation obstructed pore surfaces and restricted the reactant transport.

Lee et al. [32] investigated the effect of fabrication method on GDL porosity. The GDL was fabricated via spraying, rolling and screen methods. Sprayed and screen-printed GDL showed better performance than rolled gas diffusion layer due to their good porous structure and better gas permeability.

The influence of carbon powder in GDL was examined by Antolini et al. [33]. Two different types of carbon powders (Vulcan XC-72R and Shawinigan) were used in both gas diffusion and catalyst layers. The Shawinigan carbon powder showed better performances.

In some studies [34-36], a hydrophobic microporous sublayer, which was sandwiched between carbon cloth or carbon paper and the catalyst layer, was used to improve the electrode performance. The sublayer is supposed to improve the transport mechanism between backing and catalyst layer, and to enhance water management. Song et al. [36] constructed a microporous sublayer, which was located between catalyst layer and a wet-proofed carbon paper, by using PTFE and carbon powder. The best performance of PEMFC electrode was obtained when the carbon powder loading of the microporous sublayer was 3.5 mg/cm^2, with a 30wt% PTFE.

Kong et al. [37] investigated the effect of GDL pore-size distribution on mass-transport. The GDL was prepared from a mixture of carbon powder, isopropyl alcohol and lithium carbonate as a pore former. This mixture was directly deposed on the carbon cloth. The microporous structure was modified by adding various amounts of pore former under heat treatment at 350°C. It was reported that the pore-size distribution had more influence than the total porosity on PEMFC performance. The optimal amount of pore former was 7mg/cm^2 with 5mg/cm^2 of carbon loading in the diffusion layer and 0,4mg/cm^2 platinum loading in the catalyst layer. It was also reported in the literature [38] that additional porosity could be obtained in PEMFC electrode by adding pore former. Additional coarse porosity helps the discharging of water

from the electrode. Hence, oxygen penetrates more easily into the electrode, and consequently, improves the catalyst utilization.

The effect of GDL morphology on PEMFC performance was also investigated by Jordan et al. [39, 40]. A homogeneous suspension of carbon powder (Vulcan XC-72R or Acetylene Black) and PTFE was applied to a wet proofed carbon paper in order to form the GDL. It was reported that GDL thickness, PTFE content and GDL morphology have significant effect on the water management of PEMFC electrode. They found that acetylene black carbon showed better performance than Vulcan XC-72R carbon. This is due to the adequate porosity of acetylene black to remove water from the MEA.

Prasanna et al. [41] studied the effects of GDL properties on PEMFC performance. The GDL was prepared by using some commercial carbon papers with different physical properties based on the thickness, pore size distribution, electronic resistance, hydrophobicity and air-permeability. They noted that the gas permeability and the pore size diameter of GDL are the most important parameters in cell performance compared to other features. It was also reported that larger average pore size (above 60μm) affects negatively the cell performance because large pores show more flooding than the smaller ones due to the formation of water droplets at the interface of the GDL and the catalyst layer. Best cell performance was attained at 20wt% of Nafion content in the GDL.

Williams et al. [42] studied the critical properties of five commercial GDL and one in-house GDL at different operating conditions to determine the factors limiting oxygen transport in the cathode GDL. Limiting current, electronic resistivity, fraction of hydrophobic pores, gas permeability, pore size distribution and surface morphologies of GDL were compared each other. Beaziger et al. [43] examined the water management in GDL. Several experiments were done with commercial GDL at different Teflon loading in order to find the minimum pressure for overcoming the surface energy at the water/Teflon interface to ensure the flow through the GDL. It was reported that a few percent of large pores is enough for liquid water transportation. Smaller pores remain free for reactant diffusion from the bipolar plate to the membrane.

M.Glora et al. [44] investigated the integration of carbon aerogels in PEMFC. The GDL was constructed from resorcinol-formaldehyde (RF) aerogel films. RF films were reinforced with organic polyacrylnitril (PAN) fibers, Novoloid fibers and carbon fiber fleeces. The thickness of developed films was between 200-500μm. These films are incorporated to decrease the contact electrical resistance between the GDL and the electrolyte, as well as the bipolar plate. The highest achieved electrical conductivity was around 28 S/cm for 80% porous sample. The largest pore size was in the range of several microns. The developed GDL was tested in a single fuel cell stack and the obtained power density was 6 times lower than that of the commercial electrodes. However, they attributed this result to the poor catalyst layer preparation and not the GDL.

1.4.4 PEMFC Electrode Design

In this section, the conventional fabrication techniques of PEMFC electrodes are reviewed. Four main techniques have been used to fabricate electrodes: PTFE-bound method, thin-film method, vacuum deposition method, and electro-deposition method. These techniques are generally differentiated by the structure and the fabrication technique of the catalyst layer. Fabrication steps for each method and comparison between designs are detailed in the following section.

1.4.4.1 PTFE-Bound Technique

The PTFE-bound technique was the most used technique for PEMFC electrodes manufacturing before the invention of the thin-film technique [17, 26, 45-47]. In this method, hydrophobic PTFE is used for binding the catalyst particles. Platinum loading was decreased from $4mg/cm^2$ to $0.4mg/cm^2$ [47]. In order to ensure proton conductivity, Nafion is also impregnated into the PTFE-bound catalyst layer by spraying or brushing.

Lee et al. [26] examined the effect of Nafion impregnation on the performance of commercial low platinum-loading PEMFC electrodes. PTFE-bound method was used to prepare the electrode. Pt loading was kept constant at $0.4 \, mg/cm^2$ and Nafion was added at different concentrations (between 0 to $2.7mg/cm^2$) by brushing technique. When the air was used as an oxidant, the PEMFC performance increased with Nafion loading up to $0.6 \, mg/cm^2$. Above this loading value, PEMFC performance significantly decreased. When pure oxygen was used as an oxidant, the optimum Nafion loading was around $1.9 \, mg/cm^2$. Further increase in Nafion loading also decreased the PEMFC performance.

Chun et al. [45] compared the PTFE-bound and thin-film techniques. PEMFC electrodes made using these techniques showed respectively a performance of 350 and $650mA/cm^2$ at 0.6 V. Fabrication steps with PTFE-bound technique is shown in Figure 1-6. Ticianelli et al. [47] (from Los Alamos National Laboratory) also used this technique to develop a low platinum loading PEMFC.

Cheng et al. [48] investigated the use of platinum in PEMFC electrodes. Two electrodes were developed via PTFE-bound or thin-film techniques. The platinum utilization in the thin-film electrode was found to be lower than the PTFE-bound electrode. They attributed the low Pt utilization to the fact that the electron conduction of many catalyst particles is impaired by some thick Nafion layers or clumps.
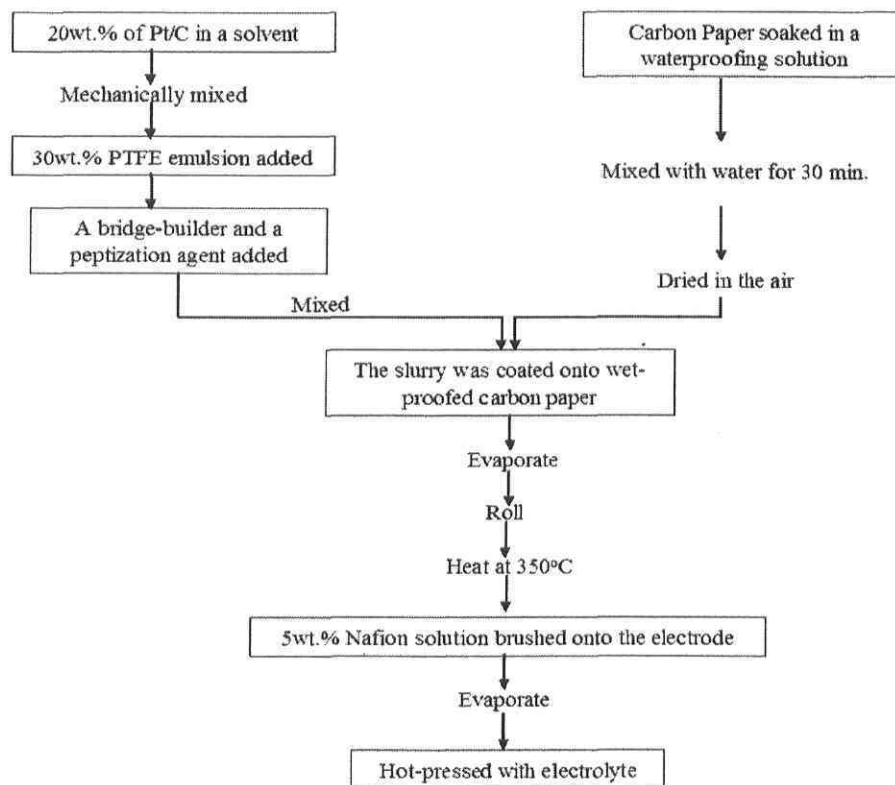
Figure 1-6 Preparation of electrode employing the PTFE-bound technique [45].

1.4.4.2 Thin-Film Technique

This technique, which was developed by Wilson [17], represents the most common fabrication technique of PEMFC electrodes. Hydrophilic perfluorosulfonate ionomer (Nafion) is used instead of hydrophobic PTFE to bind the catalyst layer. Nafion ensures the protonic conductivity and acts as a binding matrix for catalyst particles.

Thin catalyst layers are operated at a power density almost twice time higher than with PTFE-bound catalyst layers [48]. The catalyst loading was reduced below 0.35 mg/cm^2 in thin-film electrodes [17]. In addition, thin film technique is more reliable and feasible for stack fabrication [45]. A brief description of this technique, according to the Wilson's patent [17], is presented in Figure 1-7. Development of a thin-film PEMFC electrode is also presented in Figure 1-8.

5wt.% Nafion Solution + 20wt.% of Pt/C (1:3 Nafion/Catalyst ratio)

Add

Water and glycerol

Agitate the mixture with ultrasound

Nafion Electrolyte

Soak with NaOH solution

Evaporate

Apply the ink to one side of the membrane

Dry at 160°C in a vacuum

Apply the ink to other side of the membrane

Dry at 160°C in a vacuum

Subjected assembly to lightly boiling H2SO4

Rinsing in de-ionized water

Place Carbon paper/cloth

Figure 1-7 Preparation of a thin-film electrode [17].

Qi and Kaufman [49] presented a novel strategy to improve platinum utilization in PEMFC electrode. They fabricate a thin-film electrode made of 20 and 40% Pt/C at various Pt loading. Ten they boiled or steamed these electrodes at the last step of production procedure. They reported that the treatment of electrode with steam or boiling water for 10 min dramatically increase the electrode performance.

Gamburzev and Appleby [24] applied the catalyst layer onto wet-proofed carbon cloth in order to complete the thin-film electrode. Electrodes were pressed onto both sides of Nafion electrolyte. They reported three-fold improvement in cell performance at 0.7 V from 200 to 600mA/cm^2, at the same platinum loading.
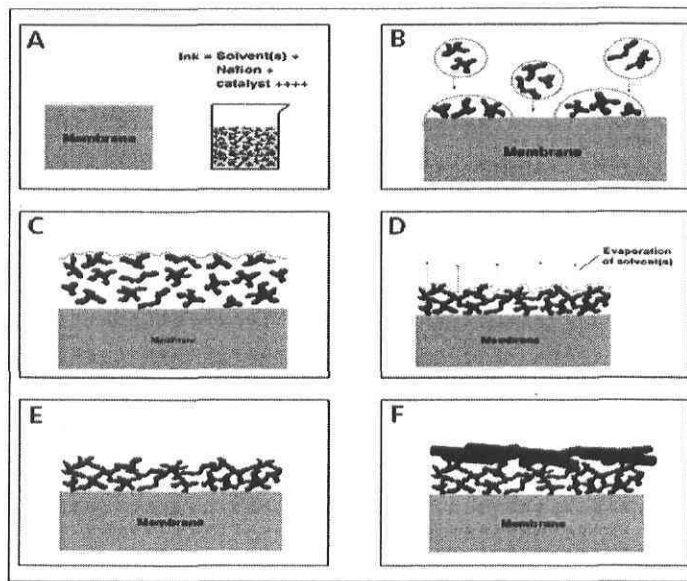
Figure 1-8 Development of a typical fuel cell electrode a) electrode formation b) ink deposition, c) film formation, d) drying the electrode, e) the dried electrode, f) application of the gas diffusion layer [50].

Passalacaua et al. [25] investigated the effects of Nafion content in the thin-film catalyst layer on cell performance and on the electrode structure. Electrodes were prepared with a Nafion content ranging from 14 to 66 wt%, while Pt content was kept constant at about 0.1 $mg.cm^{-2}$ for both anode and cathode. Optimum Nafion loading was around 33wt%. Above and below this optimum value, cell performance decreases. This case, which is presented in Figure 1-9, has been supported by several other studies [24, 27].

Song et al. [36] also studied the effect of Nafion loading on cell performance. The main difference with the other thin-film electrodes was the presence of a sublayer between the catalyst and the gas diffusion layers. The electrodes were prepared with different Nafion concentrations, varied between 0.2 and 2.0 $mg\ cm^{-2}$, while the Pt loading was fixed at 0.4 mg cm^{-2}. Optimum Nafion loading was found at 0.8 mg cm^{-2}. A sharp drop in the performance was observed above the 2.0 mg cm^{-2} of Nafion loading. This sharp drop in performance is due to the high amount of Nafion, which blocked the pores and the hydrophilic nature of Nafion that holds the water in the catalyst layer.
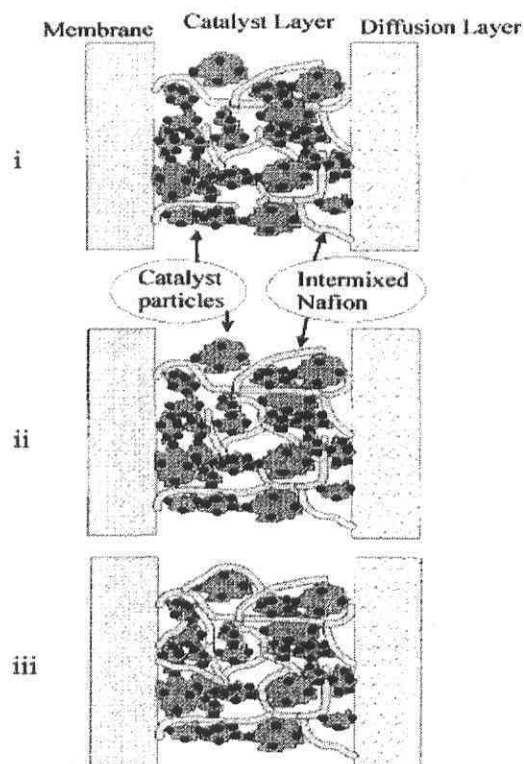
Figure 1-9 Schematic planar representation of the catalyst layer. i) Low Nafion content: not enough catalyst particles with ionic connection to membrane. ii) Optimal Nafion content: electronic and ionic connections well balanced. iii) High Nafion content: catalyst particles electronically isolated from diffusion layer [25].

The effect of several carbon blacks and graphite on PEMFC performance was studied by Passalacaua et al. [51]. Different electrodes were prepared by using thin-film technique and different grades of carbon based materials were used for GDL. The Pt loading was maintained constant at about 0.13 mg cm^{-2} for all the electrodes. The same electrode was used for both cathode and anode sides. High performance at high current density was attained by increasing the specific pore volume of the carbon black. Shawiningan Acetylene Black gave the best performance due to its high pore volume and small average pore size.
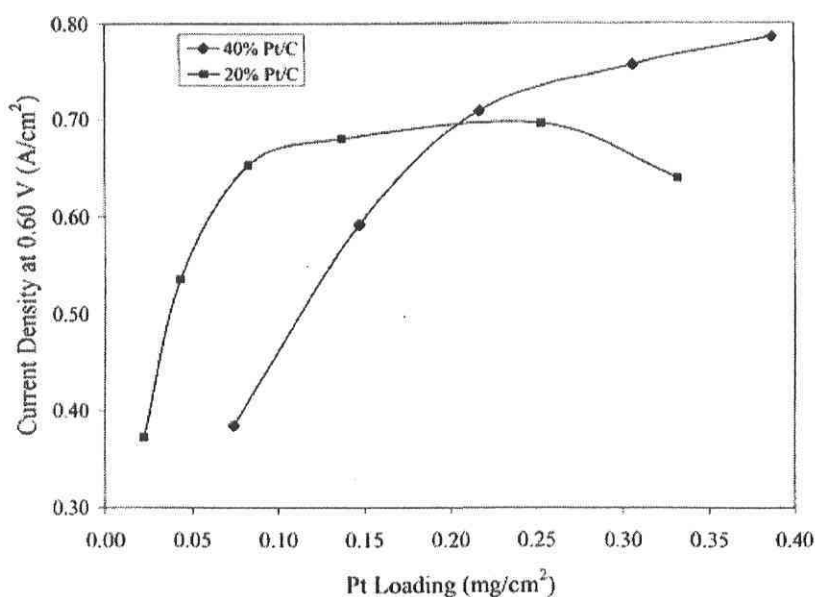
Figure 1-10 Current density at 0.6 V versus Pt loading for electrodes made using E-TEK 20 and 40% Pt/C, respectively [27].

Qi and Kaufman [27] prepared a low Pt loading high performance cathodes for the PEMFC. Carbon-supported catalysts were directly mixed with Nafion without adding any organic solvents. The viscous mixture was directly applied onto the GDL in order to form the electrode. They investigated the operating temperature effect on the fuel cell performance and reported that power density increased linearly with the cell temperature. The highest power density achieved at 75°C was 0.72 W/cm^2. They achieved maximum performance with platinum loading of 0.2 ±0.05 and 0.3 ±0.05 mg/cm^2 for 20 and 40% Pt/C, respectively (see Figure 1-10).

German Aerospace Research Establishment (DLR) research group [52-55] developed a new dry technique for fabricating membrane electrode assembly for the PEMFC. The main idea in their new technique was to spray a dry catalyst layer, prepared with either PTFE or Nafion, directly onto the membrane to avoid waiting times for evaporating solvents. Coated-membrane was hot rolled or pressed on the GDL. The main advantage of their technique was the solvent-free coating of the electrodes, which allows a continuous production of membrane electrode assembly. Furthermore, the platinum loading in the electrode was around 0.08 mg/cm^2.

1.4.4.3 Vacuum Deposition Technique

There are three common vacuum deposition techniques: chemical vapor deposition, physical or thermal vapor deposition, and sputtering deposition. Among these techniques, sputtering deposition is the most widely used method to form the catalyst layer on either the gas diffusion layer or the membrane. This technique consists of a vacuum evaporation process that removes portions of a coating material and deposits a thin and resilient film of the target material onto adjacent substrate (Figure 1-11). It provides denser catalyst layer than the other evaporation techniques [56]. By using the sputtering technique, it is possible to reduce the Pt loading in catalyst layer to around $0.01 mg\ cm^{-2}$ with maintaining good PEMFC performance.

Mukerjee et al. [57] developed PEMFC electrodes, with and without a sputtered catalyst layer, to compare the cell performance at different temperatures and pressures. They reported that current density, at $95^{o}C$ and 5 atm, of sputtered electrodes is 3.9 fold more than that of unsputtered electrodes. This improvement was attributed to the electrochemically-active surface area of the sputtered electrode, which is two times higher than that of unsputtered electrode.

Hirano et al. [58] used sputtered deposition technique to prepare an ultra low Pt loading electrode. Various amounts of Pt (between 0.04-0.3 mg Pt/cm^2) were sputtered on uncatalyzed GDL to create a cathode electrode. A commercial electrode was used for the anode part of electrode. The electro-catalyst layers of both anode and cathode were impregnated with Nafion (0.6 mg/cm^2) to ensure protonic conductivity. Cell performance with a sputtered Pt loading of 0.1 mg/cm^2 was nearly equivalent to that of the commercial variant.

O'Hayre et al. [19] developed a sputtered catalyst layer at ultra-low Pt loading by using Nafion 117 electrolyte. Catalyst layers of 5-10 nm thick produced the best PEMFC performance. This corresponds to Pt loading of around 0.01-0.02 mg/cm^2. PEMFC performance decreased dramatically when the thickness of sputtered catalyst layer is thinner than 5nm or thicker than 10nm due to the changes in the layer morphology
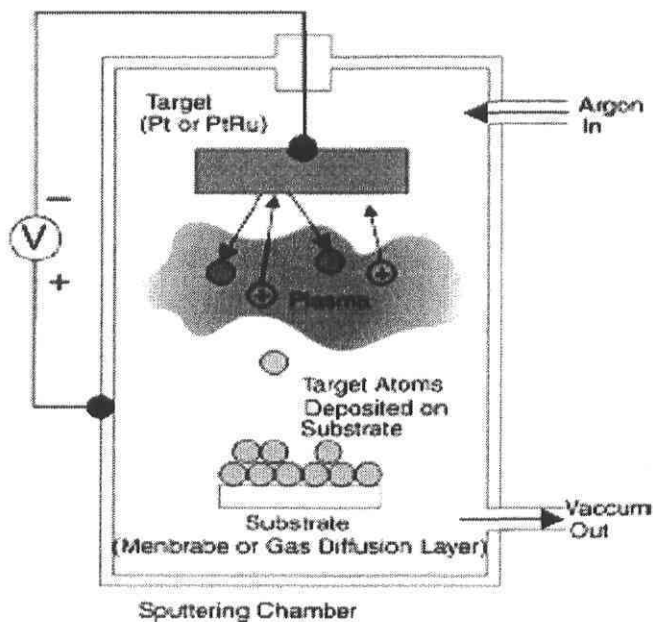
Figure 1-11 Schematic representation of sputtering deposition technique [8].

1.4.4.4 Electro-Deposition Technique

Reddy et al. [59] reported the first electro-deposition technique for the catalyst layer in PEMFC. Low platinum loading electrodes were developed by electro-deposition of Pt into uncatalyzed carbon substrate in a commercial plating bath. The uncatalyzed carbon substrate was constituted by a hydrophobic porous carbon paper, which was impregnated with PTFE and carbon powder. Nafion was also impregnated onto the uncatalyzed carbon substrate. This method is able to construct a PEMFC electrode with a platinum loading of $0.05mg/cm^2$. This low platinum loading electro-deposition electrode shows nearly the same performance with the PTFE-bound electrode with a platinum loading of $0.5mg/cm^2$.

Choi et al. [60] prepared PEMFC electrode by pulse electro-deposition method, as shown in Figure 1-12. They investigated the effect of the current density, duty cycle, and frequency during the electro-deposition process on the fuel cell performance. In the electro-deposition

cell, different electrodes were fabricated with changing the current density from 10 to $50mA/cm^2$, the duty cycle from 15 to 50%, and the frequency from 0 to 20Hz. They found the optimum current density at $25mA/cm^2$. It was also reported that, at a deposition current density of $50mA/cm^2$, the optimum conditions of pulse electro-deposition were 100 ms on-time and 300 ms off-time, and the performance of the electrode was $320mA/cm^2$ at 0.7V.
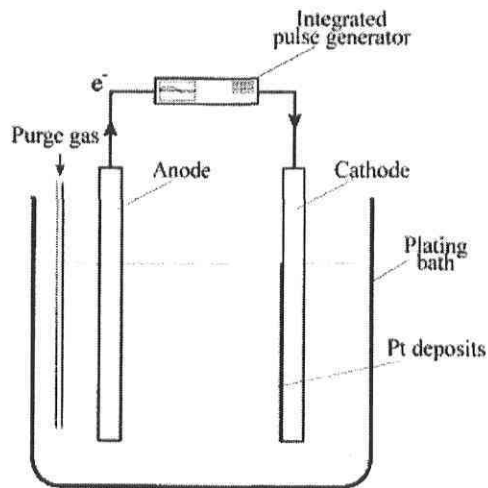
Figure 1-12 Schematic representation of electro-deposition cell [60].

1.5 PROJECT OBJECTIVES AND STRATEGY

The main objective of this project is to develop a new concept of high performance and low-cost gas diffusion layer, GDL, for PEMFC. Novel and industrially viable processing techniques, based on twin-screw extrusion process followed by post-extrusion stretching or post-extrusion selective dissolution techniques, are used. These techniques could be a good alternative to produce GDL for PEMFC.

This thesis is organized in four chapters and appendix, as described below:

The first chapter gives an introduction to fuel cell technologies, in particular that of PEMFC. The basic reactions, main characteristics and manufacturing techniques for the different fuel cell types are reviewed.

Chapter 2 concerns the development a highly conductive porous film structure for GDL by using continuous extrusion process followed by a post-extrusion stretching step. Experimental details on the different steps of GDL fabrication and characterization are described.

In Chapter 3, a second processing technique is used. The GDL is made from a matrix composed of two immiscible polymers filled with a mixture of electronic conductive materials via twin-screw extrusion process followed by selective extraction of one of the two polymers. The morphology of the porous structures is then analyzed by scanning electron microscopy, SEM, and by BET (Brunauer, Emmett, and Teller) surface area measurements.

Chapter 4 presents some conclusions related to the project and some suggestions for further investigation.

Finally, the experimental devices are presented in the appendix section.

REFERENCES

[1] Gregor Hoogers, Fuel Cell Technology Handbook, CRC press LLC, New York, 2003.

[2] Grubb, W. T.; Niedrach, L. W. J. Electrochem. Soc., 107 (1960), 131.

[3] The U.S.Department of Energy, National Energy Technology Laboratory, Fuel Cell Handbook, 5th Edition, October 2000.

[4] A.J. Appleby, F.R. Foulkes, Fuel Cell Handbook, Van Nostrand Reinhold, New York, 1983.

[5] J. Bockris, S. Srinivasan, "Fuel Cells, Their Electrochemistry, 1st Ed." McGraw-Hill, New York, 1969.

[6] S. Srinivasan, E. Ticianelli, C. Derovin, A. Redondo, J. Power Sources, 22 (1988), 359.

[7] S. Srinivasan, D. Manko, H. Koch, M. Enayetullah, A. Appleby, J. Power Sources (1990), 29, 367.

[8] S. Litster, G. McLean, J. Power Sources, 130 (2004), 61.

[9] P.D. Beattie, V.I. Basura, S. Holdcraft, J. Electroanal. Chem., 468 (1999), 180.

[10] G. Alberti, M. Casciola, Solid State Ionics, 145 (2001), 3.

[11] F. Mighri, M.A. Huneault, M.F. Champagne, Polym. Eng. Sci., 44 (2004), 1755.

[12] A. Hermann, T. Chaudhuri, P. Spagnol, Int.J. Hydrogen Energy, 30 (2005), 1297.

[13] V. Mehta, J.S. Cooper, J. Power Sources, 144 (2003), 32.

[14] M.H.Oh, Y.S.Yoon, S.G.Park, Electrochim. Acta, 50 (2004), 777.

[15] P. Costamagna, S. Srinivasan, J. Power Source, 102 (2001), 253.

[16] G.S. Kumar, M. Raja, S. Parthasarathy, Electrochim. Acta, 40 (1995), 285.

[17] US Patent, 5234777 (1993), M.S. Wilson.

[18] S.Y. Cha, W.M. Lee, J. Electrochem. Soc., 146 (1999), 4055.

[19] R. O'Hayre, S-J. Lee, S-W.Cha, F.B. Prinz, J. Power Sources, 109 (2002), 483.

[20] M.S. Wilson, J.A. Valerio, S. Gottesfeld, Electrochim. Acta, 40 (1995), 355.

[21] R.B. Moore, K.M. Cable, T.L. Croley, J. Membr. Sci., 75 (1992), 7.

[22] Y.-G. Yoon, G.-G. Park, T.-H. Yang, J.-N. Han, W.-Y. Lee, C.-S. Kim, Int. J.Hydrogen Energy, 28 (2003), 657.

[23] V.A. Paganin, E.A. Ticianelli, E.R. Gonzalez, J.Appl. Electrochem., 26 (1996), 297.

[24] S. Gamburzev, A.J. Appleby, J. Power Source, 107 (2002), 5.

[25] E. Passalacqua, F. Lufrano, G. Squadrito, A.Patti, L.Giorgi, Electrochim. Acta, 46 (2001), 799.

[26] S.J. Lee, S. Mukerjee, J. McBreen, Y.W. Rho, Y.T. Kho, T.H. Lee, Electrochim. Acta, 43 (1998), 3693.

[27] Z. Qi, A. Kaufman, J.Power Sources, 113 (2003), 37.

[28] G. Sasikumar, J.W. Ihm, H. Ryu, Electrochim. Acta, 50 (2004), 601.

[29] L. Giorgi, E. Antolini, A. Pozio, E.Passalacqua, Electrochim. Acta, 43 (1998), 3675.

[30] W.K. Lee, C.H. Ho, J.W. Van Zee, M. Murthy, J. Power Sources, 84 (1999), 45.

[31] C. Lim, C.Y. Wang, Electrochim. Acta, 49 (2004), 4149.

[32] H-K. Lee, J-H. Park, D-Y. Kim, T-H. Lee, J. Power Sources, 131 (2004), 200.

[33] E.Antolini, R.R.Passos, E.A.Ticianelli, J. Power Sources, 109 (2002), 477.

[34] Z. Qi, A. Kaufman, J. Power Sources, 109 (2002), 38.

[35] F. Lufrano, E. Passalacqua, G. Squadrito, A. Patti, L. Giorgi, J. Appl. Electrochem., 29 (1999), 445.

[36] J.M. Song, S.Y. Cha, W.M. Lee, J. Power Sources, 94 (2001), 78.

[37] C.S. Kong, D-Y. Kim, H-K. Lee, Y-G. Shul, T-H. Lee, J. Power Sources,108 (2002), 185.

[38] A. Fischer, J. Jindra, H. Wendt, J. Appl. Electrochem., 28 (1998), 277.

[39] L.R.Jordan, A.K.Shukla, T.Behrsing, N.R.Avery, B.C.Muddle, M.Forsyth, J. Appl. Electrochem., 30 (2000), 641.

[40] L.R. Jordan, A.K. Shukla, T. Behrsing, N.R. Avery, B.C. Muddle, M. Forsyth, J. Power Sources, 86 (2000), 250.

[41] M. Prasanna, H.Y. Ha, E.A. Cho, S.-A. Hong, I.-H. Oh, J. Power Sources,131 (2004),147.

[42] M.V. Williams, E. Begg, L. Bonville, H.R. Kunz, J.M. Fenton, J. Electrochem. Soc. 151 (2004), 1173.

[43] J. Benziger, J. Nehlsen, D. Blackwell, T. Brennan, J. Itescu, J. Membr. Sci., 261 (2005), 98.

[44] M. Glora, M. Wiener, R. Petricevic, H. Probstle, J. Fricke, J. Non-Cryst. Solids, 285 (2001), 283.

[45] Y.G. Chun, C.S. Kim, D.H. Peck, D.R. Shin, J. Power Sources, 71 (1998), 174.

[46] O.J. Murphy, G.D. Hitchens, D.J. Manko, J. Power Sources, 47 (1994), 353.

[47] E.A. Ticianelli, C.R. Derouin, A. Redondo, S. Srinivasan, J. Electrochem. Soc., 135 (1988), 2209.

[48] X. Cheng, B. Yi, M. Han, J. Zhang, Y. Qiao, J. Yu, J. Power Sources, 79 (1999), 75.

[49] Z. Qi, A. Kaufman, J. Power Sources, 109 (2002), 227.

[50] E. Middelman, Fuel Cell Bulletin (November 2002), 9.

[51] E. Passalacqua, G. Squadrito, F. Lufrano, A. Patti, L. Giorgi, J. Appl. Electrochem., 31 (2001), 449.

[52] D. Bevers, N. Wagner, M.V. Bradke, Int. J. Hydrogen Energy, 23 (1998), 57.

[53] E. Gulzow, M. Schulze, N. Wagner, T. Kaz, A. Schneider, Fuel Cell Bulletin No.15, 8.

[54] E. Gulzow, T. Kaz, J. Power Sources, 106 (2002), 122.

[55] E. Gulzow, M. Schulze, N. Wagner, T. Kaz, R. Reissner, G. Steinhilber, A. Schneider, J. Power Sources, 86 (2000), 352.

[56] US Patent, 6300000 (2001), C.A. Cavalca, J.H. Arps, M. Murthy.

[57] S. Mukerjee, S. Srinivasan, A.J. Appleby, Electrochim. Acta, 38 (1993), 1661.

[58] S. Hirano, J. Kim, S. Srinivasan, Electrochim. Acta, 42 (1997), 1587.

[59] N.R.K. Vilambi Reddy, E.B. Anderson, E.J. Taylor, US Pat. No. 5,084,144, 1992.

[60] K.H. Choi, H.S. Kim, T.H. Lee, J. Power Sources, 75 (1998), 230.

CHAPTER 2

Electronic Conductive Microporous Polymer Based Structures

This study aims at developing highly electronic conductive microporous structure from thermoplastic polymers filled with carbon black and graphite. The matrix was a low viscosity polypropylene, PP, and the conductive additives were composed of high specific surface area carbon black and synthetic flake graphite. Conductive blends were first prepared in a co-rotating twin-screw extruder and subsequently extruded through a sheet die to obtain films of around 500 microns in thickness. These films were then stretched in two successive steps to generate a film (100-200 microns) of controlled micro-porous structure.

2.1 INTRODUCTION

Uniaxial or biaxial stretching is a well known technique to generate porous structures in polymer films without using any solvent. Open-cell porous films having an average pore size varying from 0.05 to 2 microns have been manufactured from polypropylene, PP [1, 2] and polytetrafluoroethylene, PTFE [3] Zhu et al.[4] developed microporous PP membranes by using biaxial stretching process. They reported 30-40% porosity and 0.05μm average pore size for developed PP membranes. Chandavasu et al. [5] and Xanthos et al. [6] also developed microporous structures via post-extrusion drawing of PP-based blends. The PP matrix phase was blended by twin-screw extrusion with less than 15 wt% of polyethylene terephthalate, PET, or polystyrene, PS. The developed blends were extruded through a sheet die then uniaxially stretched. Below the glass transition temperature of the minor PET or PS phases, high local stresses generated at the interface with the PP matrix initiate the formation of micro-cracks upon stretching due to the weak adhesion between the PP/PET or PP/PS systems. The growth of these micro-cracks lead to microporous structures with pore sizes ranging from 2 to 25 nanometers.

To the best of our knowledge, there are no attempts to manufacture, by a continuous process, such as extrusion, electronic conductive porous polymer-based film structures filled with solid conductive additives. These structures are very useful for many technological applications, such as electrode gas diffusion layer for proton exchange membrane fuel cells, PEMFC. However, most polymers are known as electrically insulating materials [7-9] and their electronic conductivity can be improved by adding conductive fillers, such as carbon black, graphite, carbon fibers, or fine metallic powders. Presently, carbon based materials are the most used fillers due to their relatively lower cost, compared to noble materials, such as chrome and platinum. Adding conductive fillers at low concentrations, less than what is commonly called percolation concentration, doesn't change the conductivity of the polymer matrix. Above this percolation concentration, the conductivity increases considerably due to the interconnected conductive pathway generated by the conductive fillers [7, 10, 11]. Further increase in filler concentration above the percolation threshold leads to further small increase

in conductivity, which is important for many technological applications, such as bipolar plates or electrodes for PEMFC.

During the last few years, highly conductive polymer formulations have been developed in order to be used PEMFC technology as bipolar plates [12-15]. Highly loaded blends with up to 60wt% of conductive fillers (carbon black, graphite, and carbon fiber) were developed by twin-screw extrusion process. PEMFC bipolar plates having volume conductivity of 5 to 150 Siemens/cm were fabricated using injection or compression molding processes. The most important parameters that control blend conductivity are generally carbon black structure, such as specific surface area, processing conditions, polymer properties (morphology, crystallinity, surface tension), and selective localization of conductive fillers [7, 10, 15-22].

The main objective of this study is to produce a highly conductive porous film structure by using continuous extrusion process followed by a post-extrusion stretching step. This industrially viable technique could be a good alternative to produce electrode gas diffusion layer, GDL, for proton exchange membrane fuel cells. The GDL, which is constituted in the current technology of thin porous carbon paper, is replaced by a thin microporous layer composed of a low viscosity polypropylene, PP, containing relatively high loading of high specific surface conductive carbon black and graphite.

2.2 EXPERIMENTAL

2.2.1 Selected Materials

The thermoplastic polymer used in this study was a low viscosity PP from Basell (commercial grade SC-973 with a melt flow index, MFI = 100 dg/min). Polymer fluidity was a key factor for good processability in thin sheets of around 500μm in thickness even at high conductive additive content. Carbon black, CB, and graphite, GR, conductive additives were respectively Printex XE-2 (supplied by Degussa/Huls) and Timrex KS-75 (supplied by Timcal America). The selection of these two conductive fillers was based on a previous experimental study on conductive blends for injection-moulded bipolar plates [12]. The main carbon black and graphite characteristics in terms of conductivity/processability are their specific surface area, their surface chemistry, and their wetting properties. The main PP and conductive fillers properties are presented in Table 2-1.

Table 2-1 Characteristic properties of selected materials.

Materials	Grade	Source	Density (g/cm^3)	Melt Index [d] (dg/min)	N$_2$ Surface Area (m^2/g)
Polypropylene, PP	SC-973	Basell	0.902 [a]	100	-
Carbon Black, CB	Printex XE-2	Degussa/Huls	130 [b]	-	1000
Graphite, GR	Timrex KS-75	Timcal	0.24 [c]	-	6.5

[a] ASTM D 792.

[b] ASTM D 1513.

[c] Scott density.

[d] 230^{0}C/2.16kg.

2.2.2 Melt Compounding and Film Extrusion

Compounding at varied CB and GR filler concentrations was carried out with a 12mm diameter co-rotating twin-screw extruder (ThermoHaake Polylab system Rheomex). Optimized blends were then extruded through a flexible lip flat die to obtain 500 microns films. The barrel and die temperature setting profile was kept constant for all blends at 190/200/200°C (along the barrel) and 210°C (inside the die). The feeding rate and the rotational screw speed were also kept constant at 0.4kg/hour and 40RPM, respectively. Unfortunately, the extruder is not equipped with a calandring system to control the film thickness and thickness uniformity. To do this, a Carver hydraulic compression machine was used. The extruded films were compressed during 2 minutes (at 210°C under a force of 4 tons) inside a mould of 500 microns in thickness.

2.2.3 Rheological Characterization

The melt viscosity for all blends was measured at 230°C using high pressure capillary rheometer (Rheo-tester 1000, Gottfert). Depending on filler concentration, two capillary dies of 1 and 2mm in diameter ($L/D = 40$ for both dies) were used. Since the L/D ratio is relatively high, end effects could be neglected and no Bagley correction was done on the measured viscosity.

2.2.4 Film Resistivity Characterization

Electronic resistivity measurement was performed on films (having 20mm in length and 6-8mm in width) using an impedance analyzer (Solartron, SI 1260). The total electrical resistance, R, of the extruded films was obtained by dividing the voltage drop between the two probes by the imposed current intensity. The volume resistivity, ρ, was then obtained from the resistance, R, film thickness, t, and the width of samples, w, using the following relation:

$$\rho = \frac{R * t * w}{l} \qquad (2-1)$$

where l corresponds to the distance between the two probes.

2.2.5 Post-Extrusion Film Stretching Procedure

Optimized extruded sheets were stretched in two steps using an Instron 8821S mechanical tester equipped with a heating oven: i) The first stretching step was done at room temperature ($25^{o}C$) on $110 \times 20mm$ rectangular films in order to initiate micro-cracks at the interface between the PP thermoplastic matrix and the carbon black or graphite solid particles. ii) The second stretching step was done inside the oven at a more elevated temperature (of around $160^{o}C$) to generate thin films (100-200 μm in thickness) of controlled microporosity, as will be shown later in Figure 2-5. For PEMFC, the porous structure is needed for good mass transport of reactants (hydrogen or oxygen) from the gas flow channels to the active catalyst layer.

2.2.6 Film Morphology Characterization

The morphology of stretched films was studied on microtomed film samples using a JEOL, JSM-840 scanning electron microscope (SEM). These samples were coated with 50/50 gold-palladium alloy for SEM observations.

2.3 RESULTS and DISCUSSION

During the compounding step, the main challenges were i) to incorporate a sufficient amount of conductive particulates (carbon black and graphite) to confer good electrical conductivity, and ii) to keep blend fluidity high enough to enable film extrusion through the flat die. The apparent viscosity, at 230°C, of different PP/CB/GR blends, with varied CB/GR concentrations, is presented in Figure 2-1 as a function of the shear rate. In all blends, the composition of the conductive CB/GR additives was kept at a constant respective weight ratio of 70/30. As expected, all the blends are more viscous than the pure PP matrix over the entire range of shear rates. Blend viscosity shows a considerable increase with increasing conductive CB/GR filler concentration and shows a power law behavior. The upper curve corresponds to the maximum additive loading (35 wt%) that allowed extrusion in thin sheets using the 12mm co-rotating twin screw extruder. For an overall CB/GR additive concentration up to 35wt%, the blend viscosity is 8 to 40-fold higher than that of pure PP, depending on the shear rate. Due to the poor wetting of the solid CB/GR fillers with molten PP, a further increase of CB/GR concentration lead to processing problems, such as die blockage.

Blend composition is then a key factor to achieve an optimized film electronic conductivity (or low electronic resistivity). The main difficulty encountered during PP filling with CB and GR was to keep blend fluidity high enough to enable proper film extrusion while incorporating a sufficient amount of conductive additives to confer good electronic conductivity. Unfortunately, the PP-based blend viscosity and resistivity show opposite behaviors as the concentration of CB and GR is increased. Thus, the resistivity level is limited by the highest viscosity value at which the PP/CB/GR blend can be compounded by twin-screw extrusion process then pushed through the flat die to form thin sheets of high electronic conductivity. The big challenge in this step was to optimize between blend resistivity and film porcessability.
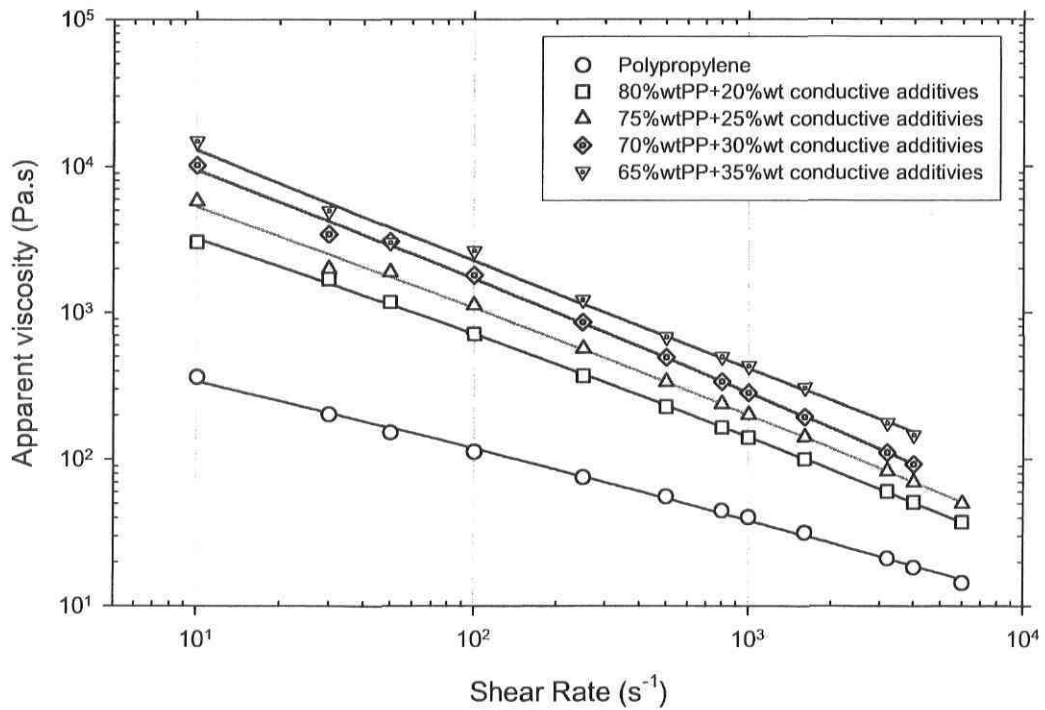
Figure 2-1 Polypropylene/Carbon Black /Graphite blends viscosity at different filler concentration at 230°C.

Figure 2-2 shows the effect of GR concentration on PP/CB/GR blend viscosity, at 230°C, for total CB/GR filler concentrations fixed at 20 and 40 wt%. For the first case, an increase in GR concentration from 6 to 10 wt% lead to a blend viscosity decrease between 1.5 to 2.0-fold, depending on the shear rate. For the second case, when GR concentration is increased from 16 to 20wt%, blend viscosity decreased by about 1.2 to 1.5-fold. Consequently, addition of GR helps to attain higher conductive concentration and yield a better processability/resistivity balance.
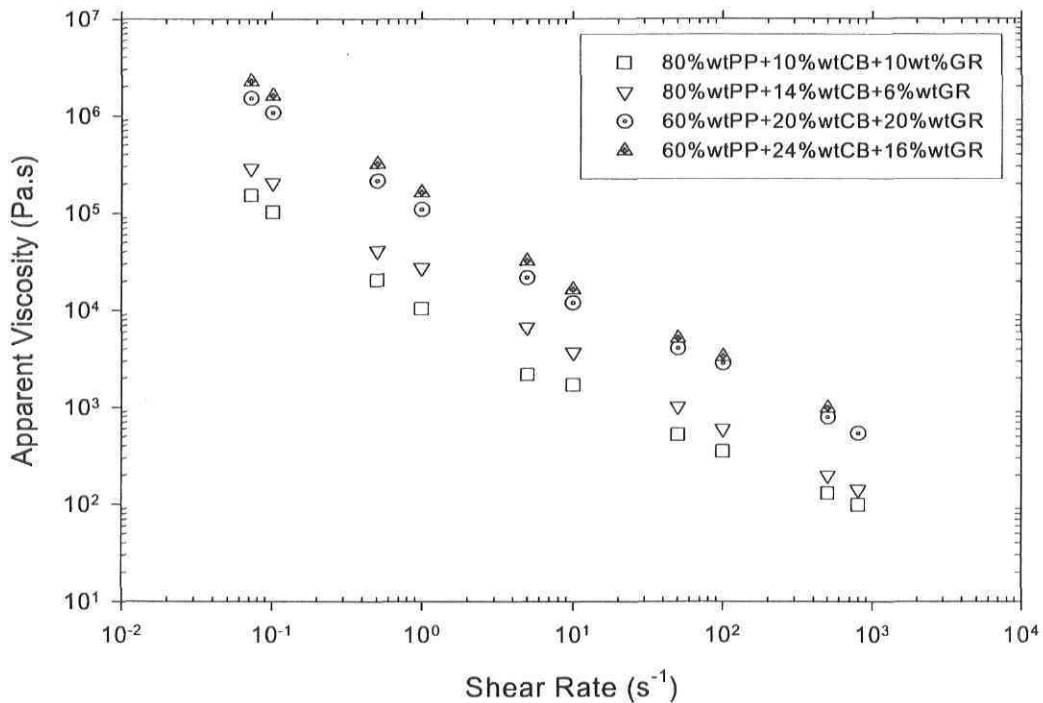
Figure 2-2 Graphite effects on the blends viscosity.

2.3.1 Film Resistivity

Resistivity measurements were done on two series of extruded films made from PP/CB/GR blends at different GB/GR concentrations. The first series correspond to extruded sheets taken directly at the exit of the die without any post-extrusion treatment, whereas the second series correspond to sheets that were compressed after extrusion, as explained in the experimental section. For both series, the composition of the conductive CB/GR additives was kept at a constant respective weight ratio of 50/50. Note that, before resistivity measurements, film surface was polished with a fine-grains polishing paper in order to remove the very thin layer of pure PP at sheet surface. Figure 2-3 presents the volume resistivity of these two series of extruded films as a function of CB/GR concentration. As expected, the resistivity decreases with increasing CB/GR concentration for both compressed and uncompressed samples. When CB/GR filler concentration is increased from 20 to 40 wt%, film resistivity is decreased by about 8-fold for uncompressed samples (from 6.4 to 0.8 Ohm-cm) and 11-fold for compressed

ones (from 2.8 to 0.2 Ohm-cm). As shown in Figure 2-3, compressed samples have lower electronic resistivity (i.e., higher conductivity) over the entire range of filler concentration. This can be attributed to the densification of the three dimensional conductive network generated by CB/GR conductive particles.
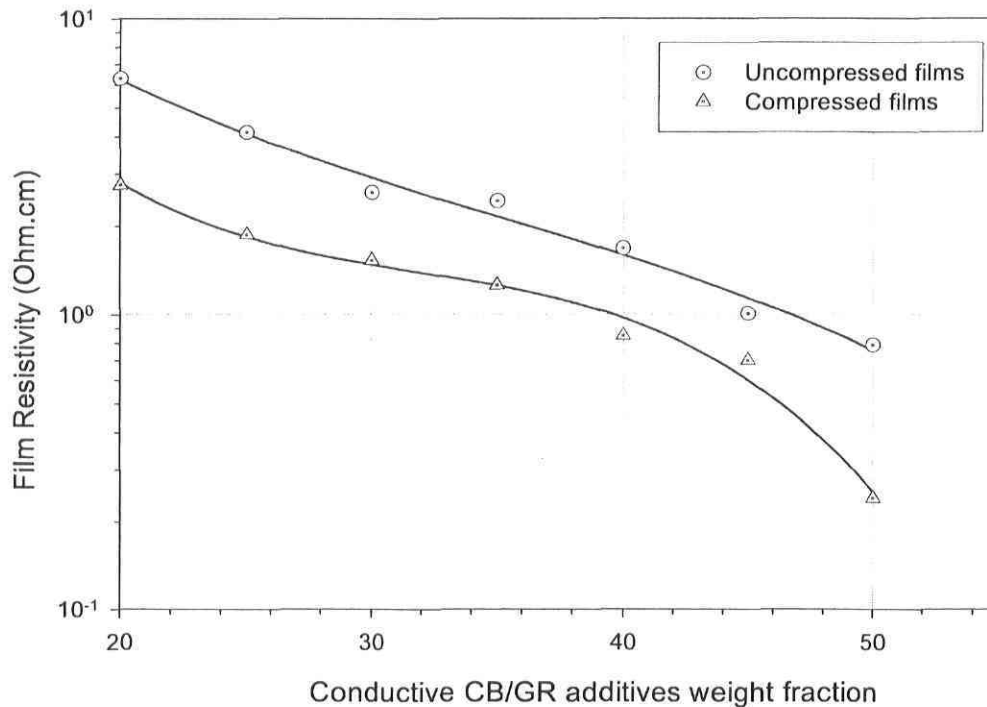
Figure 2-3 Volume resistivity for compressed and uncompressed samples at different filler concentration.

In order to compare the separate effects of carbon black and graphite on film resistivity, different resistivity measurements were done on films having the same total CB/GR filler concentration but different CB content. Figure 2-4 shows film resistivity for CB/GR total concentrations of 20, 40 and 50 wt%. For each CB/GR total concentration, the resistivity decreases when the content of CB is increased. This means that CB has a dominant effect on film resitivity due to its good electrical properties and higher specific surface area.
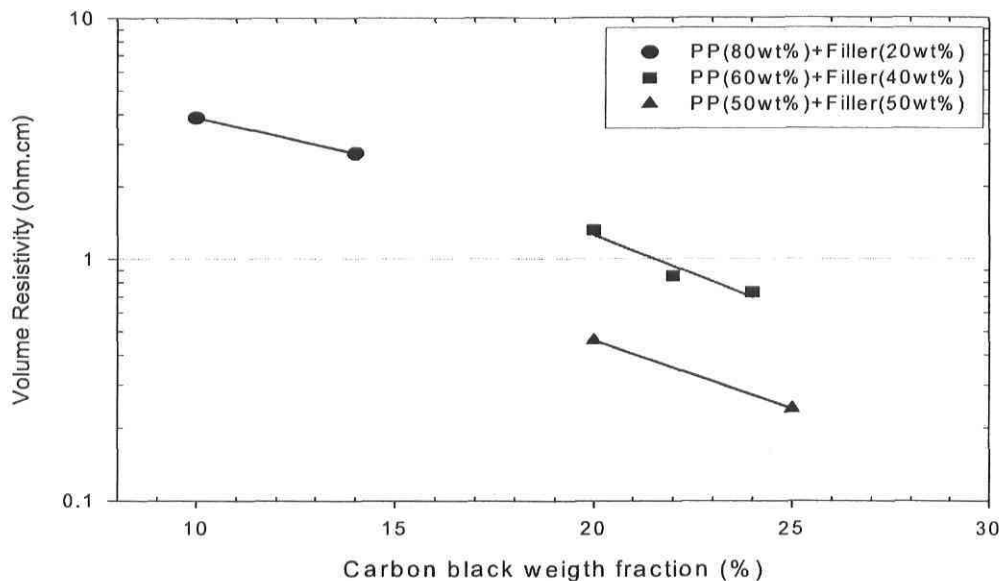
Figure 2-4 Effect of carbon black concentration on blend resistivity.

2.3.2 Film Morphology after Stretching

As explained in the experimental section, a post-extrusion stretching process under controlled conditions was done on the extruded films to generate the microporosity. These extruded films were composed of 50 wt% of PP, 25 wt% of carbon black, and 25 wt% of graphite. They were uniaxially stretched at a drawing speed of 0.2-0.5 mm/min and a stetching ratio up to 8-10% with respect to the original dimensions. Due to high CB/GR solid filler concentration, the developed films could not be stretched to higher elongation. Stretching was first carried out at room temperature to initiate micro-cracks as a result of debonding between the solid CB/GR conductive particles and the PP matrix, as sketched in Figure 2-5(b). It is expected that during film stretching, the solid dispersed phase domains composed of CB or GR act as stress concentrators. Then the high local stresses at the interface between the PP matrix and the solid CB/GR dispersed particles initiate the formation of micro-cracks upon stretching. The growth of these micro-cracks is expected to be controlled by the magnitude of the applied stress and the stretching temperature (Figures 2-5(b) and (c)).
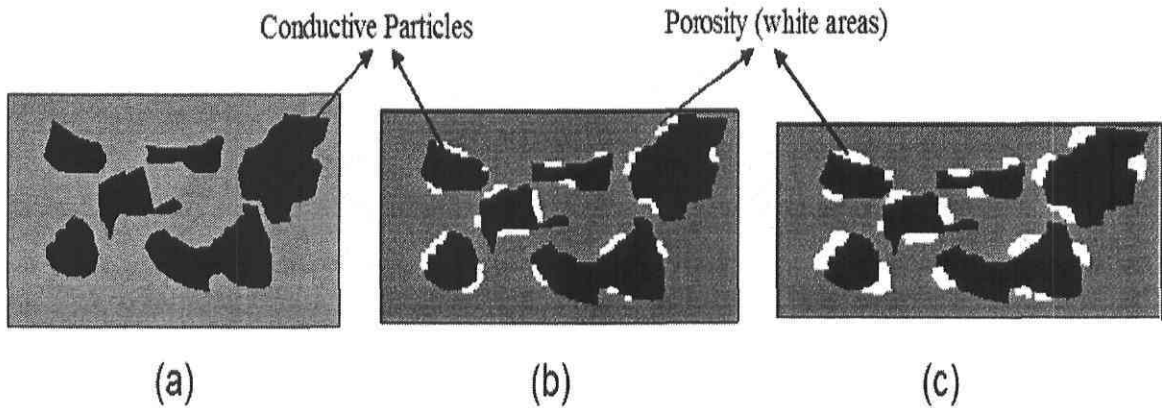
Figure 2-5 Schematic representation of micro-cracks upon stretching. **(a)** PP/CB/GR morphology before stretching **(b)** initiation of micro-cracks upon stretching at room temperature, **(c)** growth of micro-cracks upon stretching at elevated temperature (~160°C).

Figure 2-6 shows a transmission electron micrograph, TEM, of a microtomed film upon stretching in a direction parallel to the sheet surface. The extruded sheet is composed of 60wt% of PP, 22wt% of CB and 18wt% of GR. The figure shows that micro-cracks were generated due to stretching. Dark regions correspond to CB/GR dispersed domains.
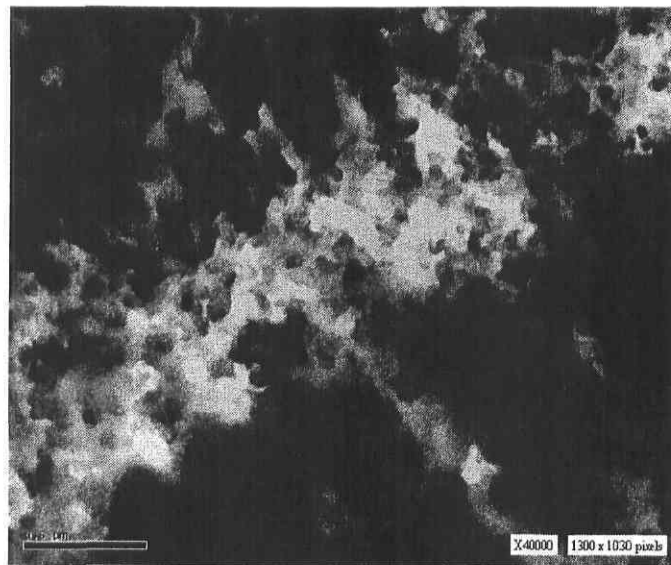
Figure 2-6 Transmission electron micrograph, TEM, of the 60PP/22CB/18GR stretched film.

2.4 CONCLUSION

In the present study, a detailed processing technique for producing electronic conductive microporous films was described. The effect of operation conditions and conductive additives on blend viscosity (processibility) and resistivity was investigated. Conductive blends were first optimized in a co-rotating twin-screw extruder and subsequently extruded through a sheet die to obtain thin sheets of around 500 microns. Optimal resistivity/processability was obtained by using a combination of high-surface-area carbon black and synthetic graphite. Good electronic resistivity of around 0.2 Ohm-cm was achieved for the optimized PP/CB/GR blend used to develop the film microporous structure. The optimized films were then stretched to generate a film micro-porous structure (100-200 microns in thickness) of high electronic conductivity. The weak interface between PP matrix and CB/GR dispersed particles was the origin of micro-cracks initiation that generates the microporosity. Work is underway to optimize the extrusion and post-extrusion processes in order to optimize the structure porosity.

REFERENCES

[1] US Patent, 5134174 (1992), M. Xu, S. Hu, J. Guan, X. Sun, W. Wu, W. Zhu, X. Zhang, Z. Ma, Q. Han, S. Liu.

[2] US Patent, 4138459 (1979), I. Brazinsky, W.M. Cooper, A.S. Gould.

[3] US Patent, 3953566 (1976), R.W. Gore.

[4] W. Zhu, X. Zhang, C. Zhao, W. Wu, J. Hou and M. Xu, Polym. Adv. Tech., 7 (1996), 743.

[5] C. Chandavasu, M. Xanthos, K.K. Sirkar, C.G. Gogos, Polymer, 43 (2002), 781.

[6] M. Xanthos, C. Chandavasu, K.K. Sirkar, C.G. Gogos, Polym. Eng. Sci., 42 (2002), 810.

[7] J.C. Huang, Adv. Polym. Tech., 21 (2002), 299.

[8] S.H. Foulger, J. Appl. Polym. Sci., 72 (1999), 1573.

[9] C. Calberg, S. Blacher, F. Gubbels, F. Brouers, R. Deltour and R. Jerome, J. Phys. D: Appl. Physics, 32 (1999), 1517.

[10] S.J. Babinec, R.D. Mussell, R.L. Lungard, R. Cieslinski, Adv. Mater., 12 (2000), 1823.

[11] I. Chodak, M. Omastova, J. Pionteck, J. Appl. Polym. Sci., 82 (2001), 1903.

[12] F. Mighri, M.A. Huneault, M.F. Champagne, Polym. Eng. Sci., 44 (2004), 1755.

[13] A. Heinzel, F. Mahlendorf, O. Niemzig, C. Kreuz, J. Power Source, 131 (2004), 35.

[14] H. Wolf, M. Willert-Porada, J. Power Source, 153 (2006), 41.

[15] R. Tchoudakov, O. Breuer, M. Narkis, Polym. Eng. Sci., 36 (1996), 1336.

[16] R. Tchoudakov, O. Breuer, M. Narkis, A. Siegmann, Polym. Eng. Sci., 37 (1997), 1928.

[17] K. Cheah, G.P. Simon, M. Forsyth, Polym. Int., 50 (2001), 27.

[18] J.G. Mallette, A. Marquez, O. Manero, R.C. Rodriguez, Polym. Eng. Sci., 40 (2000), 2272.

[19] J. Feng, C.M. Chan, Polym. Eng. Sci., 38 (1998), 1649.

[20] J.G. Mallette, L.M. Quej, A. Marquez, O. Manero, J. Appl. Polym. Sci., 81 (2001), 562.

[21] D.M. Bigg, J. Rheol., 28 (1984), 501.

[22] V. Haddadi-Asl, M. Kazacos, M.S. Kazacos, J.Appl. Polym Sci., 57 (1995), 1455.

CHAPTER 3

Development of Microporous Electrode Gas Diffusion Layer for Proton Exchange Membrane Fuel Cell, PEMFC

The aim of this work was to develop a porous film structure for electrode gas diffusion layer used for proton exchange membrane fuel cells, PEMFC. This film was made from a matrix composed of two immiscible polymers filled with a mixture of electronic conductive materials via twin-screw extrusion process followed by selective extraction of one of the two polymers. The matrix consisted of low viscosity polypropylene (PP) and polystyrene (PS) and the conductive additives were composed of high specific surface area carbon black and synthetic flake graphite. The conductive blends were first compounded in a co-rotating twin-screw extruder and subsequently extruded through a flexible film die to obtain a film of around 500 microns having high electronic conductivity. The PS phase was then extracted with tetrahydrofuran, THF, solvent and a film of controlled porosity was generated. The morphology of the porous structures was then analyzed by scanning electron microscopy, SEM, whereas the porosity characterization was done by both BET (Brunauer, Emmett, and Teller) and mercury-intrusion porosimeter. The effects of PS concentration and extraction time with THF on film porosity were also studied. Pore size distribution obtained by BET and mercury-intrusion porosimetry revealed that the GDL structure is composed by both mesopores and macropores. Mesopores represent more than 60% of the total pore volume.

3.1 INTRODUCTION

During the last few decades, a tremendous effort was undertaken to improve and commercialize the fuel cell technology especially that of proton exchange membrane fuel cells, PEMFC, because of their high energy conversion efficiency at low temperature and their zero emission feature. These characteristics assert PEMFC as an interesting option for a wide range of applications, such as transportation domain [1]. A fuel cell is an electrochemical device that continuously converts the chemical energy into electrical energy and heat via an exothermic electrochemical reaction [2]. For PEMFC, hydrogen is fed and oxidized at the anode side whereas oxygen is reduced at the cathode side, as sketched in Figure 1-2.

The membrane electrode assembly, MEA, is the hearth of the PEMFC. This layered structure, composed of two thin electrodes and one proton exchange membrane, PEM, is sandwiched between two electronically conductive bipolar plates. A typical electrode, generally less than 400μm in thickness, consists of two porous thin layers: the backing or gas diffusion layer, GDL, and the catalyst layer. Presently, the most widely used processing techniques for PEMFC electrode are the thin-film and PTFE-bound methods. In addition to these two dominant manufacturing methods, vacuum deposition (sputtering) and electro-deposition methods are also used. Most electrode designs are differentiated by the technique used to deposit the catalyst layer on the surface of carbon paper or that of carbon cloth. In PTFE-bound methods, catalyst particles are combined with hydrophobic polytetrafluoroethylene (PTFE) then cast on the GDL [3-6]. However, for thin film method, nafion (hydrophilic perfluorosulfonate ionomer) is used instead of PTFE to bind the catalyst (usually platinum). Nafion ensures the protonic conductivity inside the catalyst layer and toward the PEM. It also increases the binding quality between the electrode the membrane. These features show the performance superiority of thin film electrodes in comparison to PTFE-bound electrodes [6, 7, 8]. Compared to the last two techniques, the vacuum deposition method provides the lowest catalyst loading and thinnest electrode layers but electrode performance is slightly lower than that of conventional thin-film electrodes [9, 10].

An adequate electrode gas diffusion layer for PEMFC must be able to transport gases (hydrogen and oxygen) from the gas input channels, situated at bipolar plate surfaces, to the active area at the catalyst-membrane interface. At the same time, it must be able to transport electrons, produced and/or consumed in electrode electrochemical reactions, from the active catalyst layer to the bipolar plates that are connected to an external circuit. Presently, electrode GDL is based on porous carbon cloth or pressed carbon fibres and incorporates a hydrophobic material, such as PTFE, to create a non-wetting surface in order to prevent flooding of the GDL pores with water [8, 11]. The PTFE content should be optimized because it is not an electronic conductor and considerably reduces the GDL porosity. Giorgi et al. [12] showed that GDL porosity decreases considerably with increasing PTFE content. Glora et al. [13] developed a new category of GDL by using a resorcinol-formaldehyde aerogel. The thickness of the developed carbon aerogel films was less than 500μm and the highest achieved electronic conductivity was about 28 Siemens/cm in an 80% porous GDL structure. Pore size was in the range of several microns. However, the power density gained in their study was around 6 times lower than that of typical PEMFC. Kong et al. [14] studied the effect of GDL pore-size distribution on PEMFC electrode performance. They controlled the pore size distribution by using isopropyle alcohol and lithium carbonate, Li_2CO_3, as a pore former, together with carbon powder and PTFE. All these components were mechanically mixed then applied on a wet proofed carbon cloth. A heat treatment at 350°C is then done for the whole GDL. The use of the pore former and heat treatment lead to a higher porosity and power density. The effect of carbon black structure on PEMFC performance was studied by Antolini et al. [15]. Oil furnace carbon black (Vulcan XC-72R) or acetylene-black (Shawingan) were mixed with PTFE and cast onto carbon cloth or carbon paper with different methods. The Catalyst layer, composed of a mixture of platinum on carbon black catalyst, Pt/CB, nafion and isopropanol (as solvent) was applied by painting on the GDL surface. Best electrode performance was obtained by using acetylene-black in the GDL and Vulcan XC-72R carbon powder in the catalyst layer. Song et al. [16] developed a PEMFC electrode with the introduction of a catalyst supporting layer (composed by CB powder in PTFE matrix) located between the GDL and the catalyst layer. Their work focused on the optimization of the supporting layer. Qi et al [17] also used a supporting layer between the catalyst layer and the

carbon paper support in order to improve the water management inside the electrode. PEMFC performance was investigated at different cell and reactant (air, hydrogen) temperatures, with and without the supporting layer. An optimized PEMFC performance was achieved by using a microporous supporting layer, which contains 35wt% of PTFE and 65w% of Vulcan XC-72 carbon powder.

An important drawback of most of the materials described above, which were used for PEMFC electrodes, is that they cannot be melt-processed. However, blending thermoplastic polymers with highly conductive additives could provide alternative electrode materials that could be used in industrial and low-cost mass production processes. These materials have the advantage to be melt-processed using conventional processing techniques, such as twin-screw extrusion, and consequently, they can enhance the integration of the membrane-electrode assemblies.

Polymers filled with conductive additives, such as carbon black, carbon fibers, and graphite, have been already used in PEMFC technology, especially for bipolar plate manufacturing by injection or compression molding processes [18, 19, 20]. However, these filled polymers alone have no sufficient porosity to transport reactant gases (hydrogen and oxygen). The main objective this study is to develop a state-of-the art methodology to prepare electrode GDL by using a continuous melt extrusion process followed by a selective dissolution post-extrusion step. The GDL, which is constituted in the current technology of thin porous carbon paper, is replaced by a thin porous layer composed of a mixture low-viscosity PP and PS, filled with high specific surface conductive carbon black and graphite.

3.2 EXPERIMENAL

3.2.1 Materials

The thermoplastic polymers used in this study were a low viscosity PP from Basell (commercial grade SC-973) and two different grades of PS; the first one from Dow Chemical (commercial grade APR-615) and the second one from Nova Chemical (commercial grade PS-3900). Polymer fluidity was a key factor for optimal processability in films of around 500μm in thickness, even at high conductive additive content. Carbon black, CB, and graphite, GR, conductive additives were Printex XE-2 (supplied by Degussa/Huls) and Timrex KS-75 (supplied by Timcal America), respectively. The choice of these two conductive fillers was based on a previous experimental work on conductive blends for injection-moulded bipolar plates [18]. The main carbon black and graphite characteristics in terms of conductivity/processability are their specific surface area, their pore size distribution, their surface chemistry and wetting properties. The synthetic graphite was particularly used for its good conductivity and excellent lubricating properties. A good lubricating property provides better blend processability and allows higher CB loading. Table 3-1 presents the grade names, melt flow indices, and suppliers of PP, PS, CB and GR used in this study.

Table 3-1 The different polymers, carbon black and graphite used in this study.

Materials and their designation	Commercial name	Supplier	Density (g/cm^3)	Melt Index [d] (dg/min)	N$_2$ Surface area (m^2/g)
Polypropylene, PP	SC-973	Basell	0.902 [a]	100 [e]	-
Polystyrene, PS-1	3900	Nova Chemical	1.04	38 [f]	-
Polystyrene, PS-2	APR-615	Dow Chemical	1.04 [a]	14 [f]	-
Carbon Black, CB	Printex XE-2	Degussa/Huls	0.13 [b]	-	1000
Graphite, GR	Timrex KS-75	Timcal America	0.24 [c]	-	6.5

[a] ASTM D 792, [b] ASTM D 1513, [c] Scott density, [d] ASTM D 1238, [e] 230°C/2.16kg, [f] 200°C/5kg

3.2.2 Compounding Process

Two compounding methods were used with a 12mm diameter intermeshing co-rotating twin screw extruder (ThermoHaake Polylab system Rheomex): i) the first method consisted in one-step blending. First, PP and CB were separately dry-mixed at different concentrations with PS and GR, respectively. The two mixtures were then loaded together to the extruder by using two special gravimetric hoppers. ii) The second method consisted in two-step compounding. During the first step, only PP was mixed with the solid CB and GR additives. The obtained blend was then compounded with PS during a second step using the same extruder. Since the PS dispersed phase has to be extracted during the post-extrusion selective dissolution step, the objective was to situate the major part of the conductive CB and GR additives in the PP matrix. For both techniques, same processing parameters were used. The barrel and die temperature setting profile was kept constant for all blends at $210/225/225^\circ C$ (along the barrel) and $230^\circ C$ (inside the die). The feeding rate and the rotational screw speed were also kept constant at 0.4kg/hour and 40RPM, respectively. The optimized blends were then extruded through a flexible lip flat die to obtain films of around 500 microns in thickness. Unfortunately, the extruder was not equipped with a calandring system to control the film thickness and thickness uniformity. To do this, a Carver hydraulic compression machine was used. The extruded films were compressed during 2 minutes (at $210^\circ C$ under a force of 4 tons) inside a mould of 500 microns in thickness.

3.2.3 Rheological Characterization

The melt viscosity for all blends was measured at $230^\circ C$ using high pressure capillary rheometer (Rheo-tester 1000, Gottfert). A capillary die of 1mm in diameter ($L/D = 40$) was used. Since the L/D ratio is relatively high, end effects could be neglected and no Bagley correction was done on the measured viscosity.

3.2.4 Post-Extrusion Selective Extraction Technique

The extruded films were put during three days into tetrahydrofuran, THF, solvent at 25°C to extract the PS phase in order to generate the film porous structure. THF was used as a solvent because it doesn't dissolve PP at room temperature [21]. After PS extraction, resulting porous films were washed with acetone then dried, at 70°C, under vacuum during 12 hours.

3.2.5 Electronic Resistivity Characterization

Electronic resistivity measurements were performed along the extrusion direction (in-plane resistivity) and perpendicular to the extrusion direction (through-plane resistivity). The in-plane resistivity was measured on films (having 20mm in length and 6-8mm in width) using an impedance analyzer (Solartron, SI 1260). The total electronic resistance, R, of the extruded films was obtained by dividing the voltage drop between the two probes by the imposed current intensity. The resistivity, ρ, was then obtained from the resistance, R, the film thickness, t, and the width of samples, w, using the following relation:

$$\rho = \frac{R * t * w}{l} \tag{3-1}$$

where l corresponds to the distance between the two probes.

For through-plane resistivity measurements, a Keithley auto-ranging electrometer (Model-197) with electrode diameter of 12.6mm was used. The resistivity, ρ, was calculated according to the following relation:

$$\rho = \frac{R * \pi * D^2}{4t} \tag{3-2}$$

where, R is the total electronic resistance, D and t are the electrode diameter, and film thickness, respectively. In order to improve the contact between the electrodes and the tested samples, a conductive carbon cloth was inserted between the sample and each electrode. The electronic resistance of this carbon cloth was subtracted from the total resistance.

3.2.6 Morphology Characterization

Film morphology after the extraction of PS phase was analyzed using a JEOL, JSM-840 scanning electron microscope (SEM). Microtomed samples were coated with 50/50 gold-palladium alloy and SEM observations were done on surfaces parallel and perpendicular to the extrusion direction.

3.2.7 Porosity Characterization

After PS extraction by THF solvent, film porosity was characterized by both BET and mercury porosimetry techniques. The BET was used to determine the specific surface area and to characterize the micropores and mesopores, whereas the mercury porosimeter was used to characterize the macropores.

In the present study, surface area and pore size distributions are measured using a Micromeritics, Tristar 3000 for BET technique and Micromeritics, Poresizer 9320 for Mercury-Instrusion Technique.

3.2.7.1 BET Technique

The specific surface area, which is a measure of the porosity, was calculated by applying the BET equation (Brunauer, Emmett, and Teller [22]):

$$\frac{P}{V \cdot (P^o - P)} = \frac{1}{V_m \cdot c} + \left(\frac{c-1}{V_m \cdot c} \right) \frac{P}{P^o} \qquad (3\text{-}3)$$

where P is the vapor pressure of the gas, P^o is the equilibrium vapor pressure of the liquid, V is the volume of the gas adsorbed at pressure P and V_m corresponds to the volume of adsorbed gas at standard temperature and pressure (STP) in a monolayer, respectively. The parameter c is related to the energy of adsorption by the following relation:

$$c = \exp\left(\frac{E_1 - E_L}{RT} \right) \qquad (3\text{-}4)$$

where E_1 is the heat of adsorption in the first layer and E_L is the heat of vaporization. T and R are the temperature and the universal gas constant, respectively.

Equation 3-3 gives a linear relationship between $\dfrac{P}{V \cdot (P^o - P)}$ and $\dfrac{P}{P^o}$ from which the values

of V_m and c can be obtained from the slope $\left(\dfrac{c-1}{V_m \cdot c} \right)$ and the intercept $\dfrac{1}{V_m \cdot c}$.

The specific surface area, S, is the calculated using the following equation:

$$S = \frac{V_m \cdot N \cdot a}{v_M} \qquad (3\text{-}5)$$

where N is Avogadro's number ($N = 6.022 \times 10^{23} \ molecules/mol$), a is the area corresponding to one adsorbed nitrogen molecule ($a = 1.62 \times 10^{-19} \ m^2/molecule$), and v_M is the molar volume of the gas at STP ($v_M = 22.4 \ L/mol$).

3.2.7.2 Mercury-Intrusion Technique

The BET technique is able to determine pore sizes up to around 0.050 µm. In order to analyze the whole pore sizes generated inside the film, a second technique using a mercury-intrusion pore size analyzer was used. This technique measures the amount of mercury penetrated into pores of a porous media as a function of the applied pressure. Pressure required to penetrate mercury into a certain size of pore is a function of the pore diameter. In the present work, pore size distribution was collected using a Micromeritics Poresizer 9320, which can analyze any porous media with a pore size range between 0.050–300 µm.

3.3 RESULTS AND DISCUSSION

During the step of blend formulation by twin-screw extrusion process, the main challenge was to ensure a low blend viscosity in order to enable proper extrusion in thin films while incorporating a sufficient amount of carbon black and graphite conductive additives to confer to the extruded film a good electronic conductivity (i.e., low resistivity). Generally, the electronic resistivity of pure polymers varies between 10^{14} and 10^{18} Ohm-cm. Those of CB and GR are around 10^{-1} and 10^{-3} Ohm-cm, respectively. The electronic resistivity level for the polymer/CG/GR blends varies between these extreme values and the target resistivity values for this work must be situated in the acceptable range for PEMFC electrodes. For reference purpose, the resistivity of carbon fiber mat, which is a commercial material for PEMFC electrode gas diffusion layers, is around 2.3 Ohm-cm [23].

As shown by Mighri et al. [18], blend viscosity (which is a measure of the degree of processability) and resistivity show opposite behaviours as the conductive filler (composed by a mixture of carbon black and graphite) concentration is increased. Thus, for thin film extrusion, the target resistivity level is limited by the highest viscosity values at which the filled polymer blend could be compounded and extruded through the film die. Based on previous highly conductive formulations developed for PEMFC bipolar plates [18], PP/PS/CB/GR blend initial compositions were carefully chosen. These compositions were then optimized in order to determine the best compromise between resistivity, film processability, and film porosity. To do this, the first series of blend formulations focused on resistivity/processability optimization by determining the optimized blend composition. For porosity optimization, a second series of blend formulations were prepared in which PS concentration was carefully adjusted to get maximum film porosity (after selective extraction of the PS dispersed phase).

3.3.1 Rheological Behavior of the Developed Blends

As mentioned in section 3.2.1, the PP grade (SC-973 from Basell) was selected as the main matrix for its high fluidity and its good chemical and thermal resistance [18]. The two PS grades, PS-1 and PS-2, were studied in order to select the grade that gives the lowest blend viscosity. Two blends having the same PP, PS, CB and GR concentrations were then prepared using PS-1 and PS-2. The apparent viscosities of these two blends, at 230°C, are presented in Figure 3-1 together with those of PS-1 and PS-2. Even though PS-1 shows a lower viscosity than PS-2 over the entire range of the shear rates studied, their corresponding blend viscosities are not very different. The PS-1 based blend shows only a slight lower viscosity for shear rates higher than $50s^{-1}$, i.e., in the range of the extrusion shear rates. At these composition levels, CB and GR have a dominant effect on blend viscosity. However, PS-1 was chosen for blend formulations just for its slight lower viscosity and, particularly, for its availability in our laboratory.
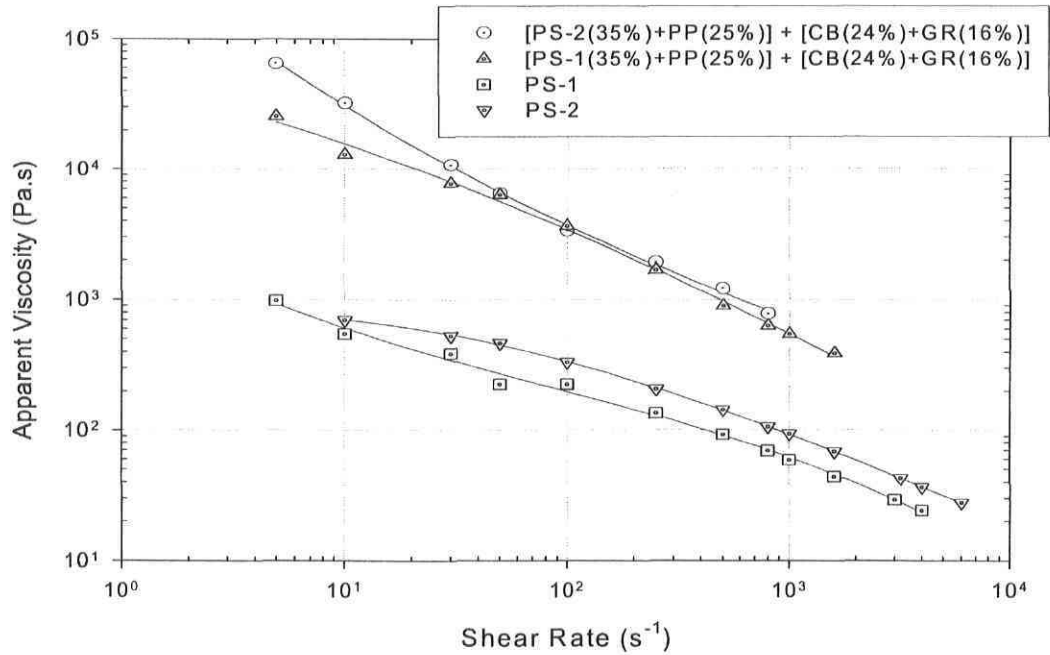
Figure 3-1 Apparent viscosity as a function of shear rate at 230°C: Pure PS-1 and PS-2 and their corresponding PP/PS/CB/GR blends of the same components concentrations.
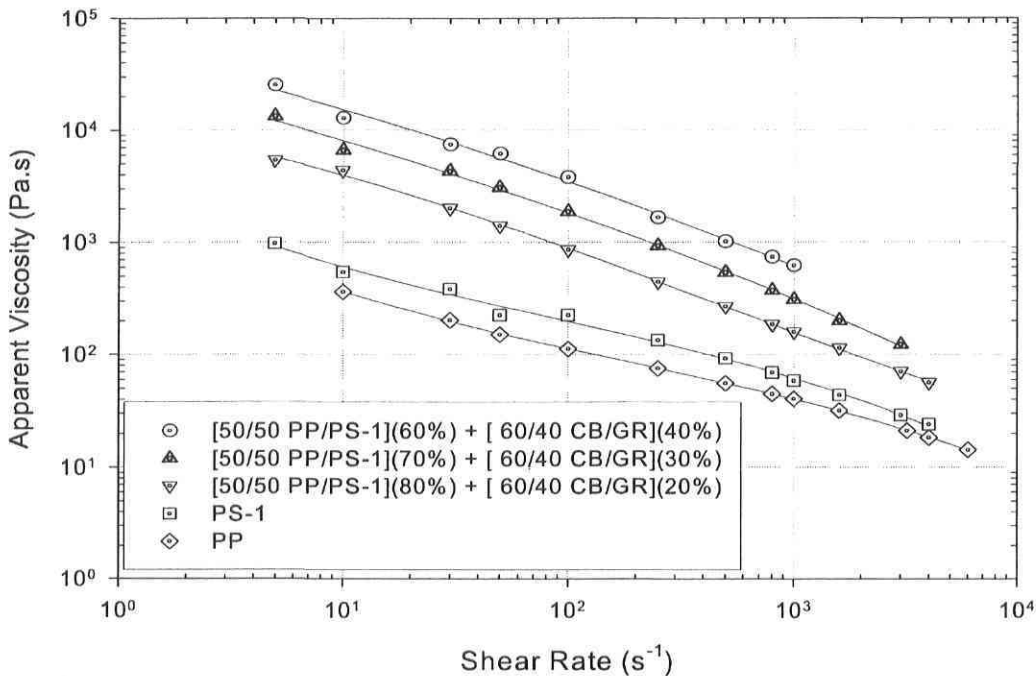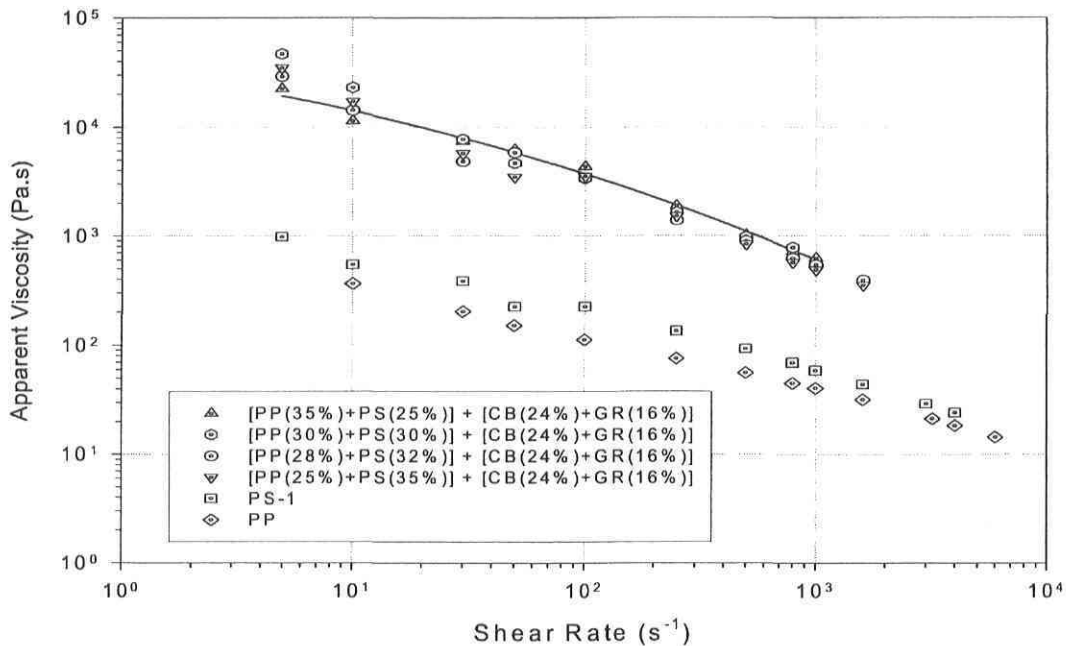
Figure 3-2 Apparent viscosity as a function of shear rate at 230°C: Pure PP and PS-1 together with three PP/PS-1/CB/GR blends. The three blends are respectively composed of 60, 70 and 80wt% of 50/50 PP/PS-1 mixtures, and 40, 30 and 20wt% of 60/40 CB/GR mixtures.

Figure 3-2 shows the apparent viscosities of pure PP and the selected polystyrene grade, PS-1, together with those of three PP/PS-1 based blends. These three blends are composed of 60, 70 and 80wt% of 50/50 PP/PS-1 mixture as polymeric phase, and respectively 40, 30 and 20wt% of 60/40 CB/GR mixture as conductive additives. Over the entire range of the shear rates studied, the three blends are more viscous than pure PP and PS-1 and blend viscosity increases with increasing the CB/GR concentration. It should be mentioned that the 40wt% of 60/40 CB/GR solid additives corresponds to the maximum loading allowed by the extruder used in this study. Due to the poor wetting of these solid additives with molten PP and softened PS-1, further increase of CB/GR concentration lead to processing problems, such as die blockage. Therefore, the blend composed of 60wt% of PP/PS-1 as polymeric phase and 40wt% of 60/40 CB/GR mixtures as a conductive additive was chosen for further conductivity/porosity

optimization. Only polymeric phase composition was changed during this optimization step; seven blends were prepared by varying the weight fraction of PS-1 from 25 to 42wt% (shown in Table 3-2). The entire PP/PS-1 polymeric phase concentration in the blend was maintained constant at 60wt%. Figure 3-3 shows the apparent viscosities of pure PP and PS-1, together with four of the seven prepared blends. As will be shown later, various PS-1 concentrations were chosen in order to determine the blend final composition that leads to a co-continuous morphology needed for optimal porosity (in order to ensure gas diffusion through the gas diffusion layer). From the viscosity (processability) point of view, Figure 3-3 shows no big difference between the different blends. Blend viscosity is much more controlled by CB/GR solid additives, especially at high shear rates.

Table 3-2 Weight concentration of components in prepared blends.

| Reference	Concentration
S-1	PP(35%) + PS(25%) + CB(24%) + GR(16%)
S-2	PP(30%) + PS(30%) + CB(24%) + GR(16%)
S-3	PP(28%) + PS(32%) + CB(24%) + GR(16%)
S-4	PP(25%) + PS(35%) + CB(24%) + GR(16%)
S-5	PP(22%) + PS(38%) + CB(24%) + GR(16%)
S-6	PP(20%) + PS(40%) + CB(24%) + GR(16%)
S-7	PP(18%) + PS(42%) + CB(24%) + GR(16%)

Figure 3-3 Apparent viscosity as a function of shear rate at 230°C: Pure PP and PS-1, together with four different PP/PS-1/CB/GR blends having identical PP/PS-1 phase and CB/GR phase concentrations. Only PS-1 concentration is varied from 25 to 35wt%.

3.3.2 Resistivity Characterization of Extruded Films

Figure 3-4 presents film in-plane and through-plane resistivities, together with their corresponding blend viscosity at a shear rate of $500s^{-1}$, as a function of CB/GR weight concentration. As in the case of Figure 3-2, polymeric phase and additive compositions of the five blends presented in the figure 3-4 were 50/50 PP/PS-1 and 60/40 CB/GR, respectively. Both in-plane and through-plane film resistivities decrease with increasing CB/GR concentration and the in-plane resistivity is considerably less than the through-plane resistivity. This is principally due to the preferential orientation of CB and especially GR flakes along extrusion direction (i.e., polymer flow direction). The decreasing rate of the through-plane resistivity is much higher than that of the in-plane resistivity. This could be attributed to the higher probability of contact between GR flakes, which causes some random orientation and, consequently, much more contact between the conductive particles across the

film thickness. As shown in Figure 3-4, an increase of CB/GR phase concentration from 20 to 40wt% leads to a substantial increase in blend viscosity (around 4-fold). Of course, the decreased resistivity only comes at a cost in term of viscosity (i.e., processability).
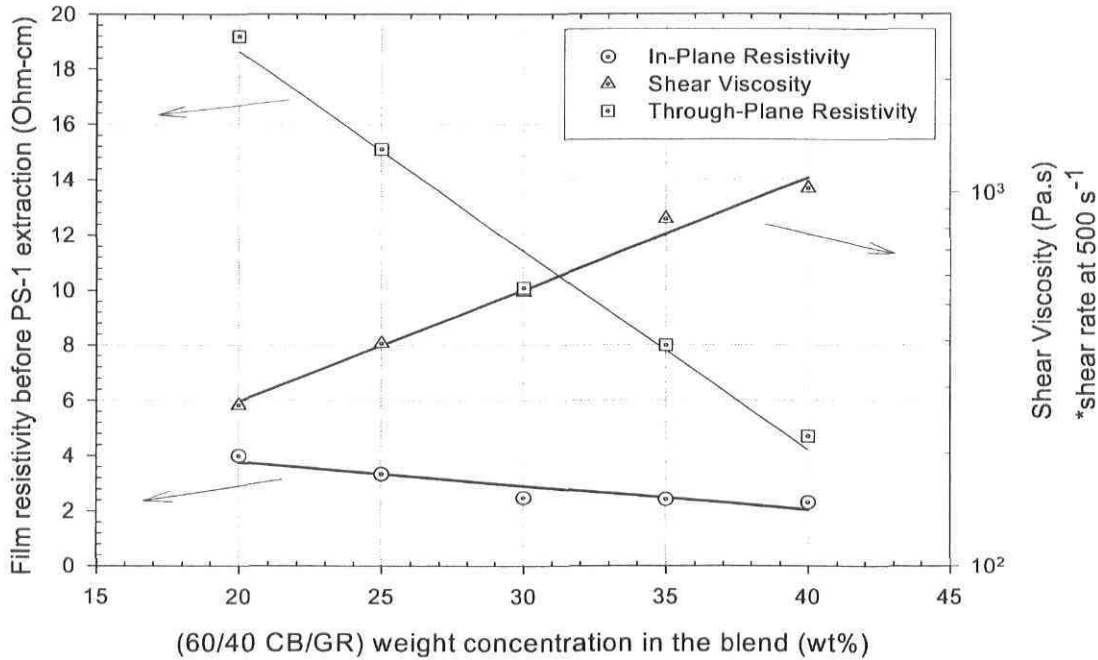
Figure 3-4 In-plane and through-plane film resistivities and their corresponding blend viscosities (at a shear rate of 500 s^{-1}) as a function of CB/GR phase concentration.

The next part of this study focuses on the effect of PS-1 concentration on both film resistivity and porosity after the extraction of PS-1 phase with THF solvent. The blend composed of 60wt% of PP/PS-1 as polymeric phase and 40wt% of 60/40 CB/GR mixtures was used. As mentioned in section 3.3.1, seven blends in which the weight fraction of PS-1 was varied from 25 to 42wt% were analyzed in order to determine the optimized PS-1 concentration that gives the lower resistivity and at the same time higher porosity. Figure 3-5 shows the in-plane and

through-plane resistivities of porous films made from these seven blends after the extraction of PS-1 phase, as a function of PS-1 weight concentration. As before PS-1 extraction, the through-plane resistivity remained higher than the in-plane resistivity. For the same blend composition 60wt% of 50/50 PP/PS-1 and 40wt% of 60/40 CB/GR, Figures 3-4 and 3-5 show that in-plane and through plane resistivities were not visibly affected by PS-1 extraction. Based on this result, it can be concluded that most of CB and GR additives were dispersed in the PP phase. This can be explained by the fact that the PP matrix is less viscous than the PS phase over the entire range of shear rates. Figure 3-5 also shows that the in-plane and through-plane resistivities vary approximately in opposite directions when PS-1 concentration is increased from 25 to 42wt%. The in-plane resistivity remains almost unchanged when PS-1 concentration is increased from 25 to 30 wt%, whereas the through-plane resistivity shows a more pronounced decrease. When PS-1 concentration is increased from 30 to around 38 wt%, the in-plane resistivity decreases from 2.2 to around 1.0 Ohm-cm but the though-plane resistivity remains approximately constant around an average value of 4.6 Ohm-cm. However, for PS-1 concentration higher than 38 wt%, the opposite variation of the in-plane and through plane resistivities becomes more evident. When PS-1 concentration is increased from 38 to 40 wt%, the in-plane resistivity increases from 1.0 to around 1.6 Ohm-cm and the through-plane resistivity decreases from 4.6 to around 3.8 Ohm-cm. Further increase of PS-1 concentration leads to a decrease of the in-plane resistivity and an increase of the through plane resistivity. Both in-plane and through-plane resistivity variation with varying PS-1 concentration can be explained in term of blend morphology.
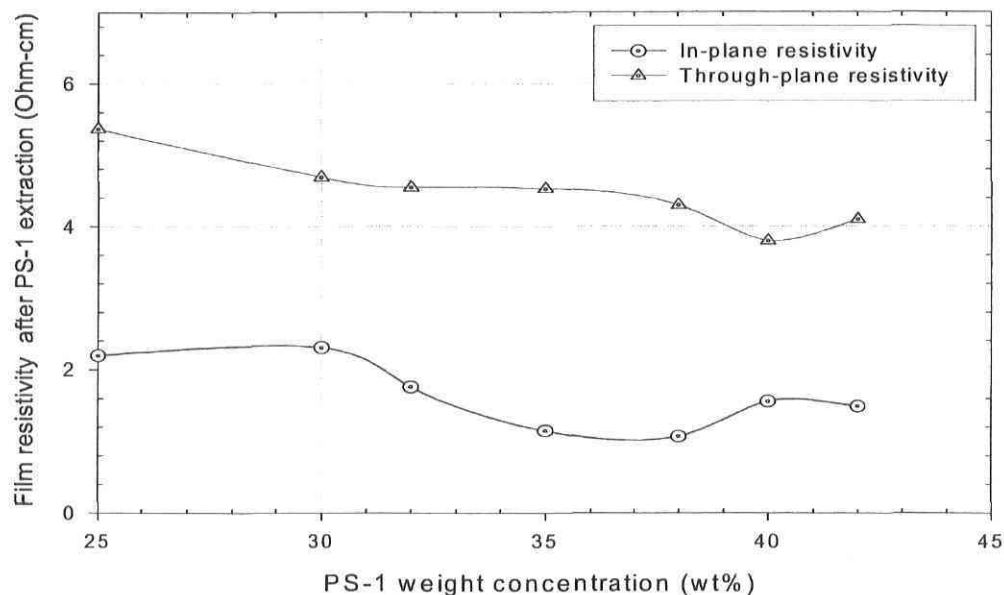
Figure 3-5 In-plane and through-plane blend resistivities of different porous extruded films after the extraction of PS-1 phase with THF solvent, as a function of PS-1 weight fraction, which was varied from 25 to 42wt%.

3.3.3 Morphology Characterization of Films after the Extraction of Polystyrene Phase by THF Solvent

To be effective, a PEMFC electrode gas diffusion layer must exhibit substantial porosity. Furthermore, the pores should be interconnected and open to the surface in order to adequately ensure gas diffusion. In order to generate film porous structure, which in our case will be composed of both mesopres and macropores, ideal film morphology should form co-continuous networks of PP matrix filled with CB/GR mixture and void spaces left by the extracted PS-1. In this case, two kinds of pore structures coexist: micro and mesoporous structure globally generated by CB and graphite network inside the PP matrix, and macroporous structure generated by void spaces left by extracted PS-1 phase. For this reason, PS-1 weight concentration was varied between 25 to 42wt% in order determine the

corresponding concentration that ensures macroporous structure co-continuity inside the film in order to ensure good diffusivity of the reacting gases through the GDL.

Figures 3-6[(a)-(e)] show SEM micrographs of 5 porous films, having different PS-1 concentrations, after three days of PS-1 extraction by THF solvent. These films were microtomed along the extrusion direction without any post-extrusion compression. For all PS-1 concentrations, the corresponding films show macroporous structures in which macropores generally had a non spherical shape. Film macroporosity (fraction of voids left by extracted PS-1) increases with increasing PS-1 weight concentration, whereas macropore size doesn't show any significant variation. Figures 3-6(c) and 3-6(d), which correspond to PS-1 concentrations of 38 and 40wt%, respectively, clearly show that macropores are highly interconnected (coalesced). However, for PS-1 concentration of 42wt% (Figure 3-6(e)), the macropores are larger and, as will be shown in the following porosity characterization section, this leads to a decrease in pore surface area.

As mentioned at the beginning of this section, the macropores should be interconnected and open to the film surface in order to ensure gas diffusion adequately. To verify if this was the case for the developed films, SEM micrographs of microtomed film samples were taken perpendicular to the extrusion direction (i.e., across film thickness) for different PS-1 concentrations (Figures 3-7(a)-(d)). These micrographs revealed that the generated macropores are interconnected across the film thickness and this interconnection is much higher than that along the extrusion direction. It was also observed that pores are open to the film surface. This means that an open cell structure was generated, which is one of the main objectives of this study.
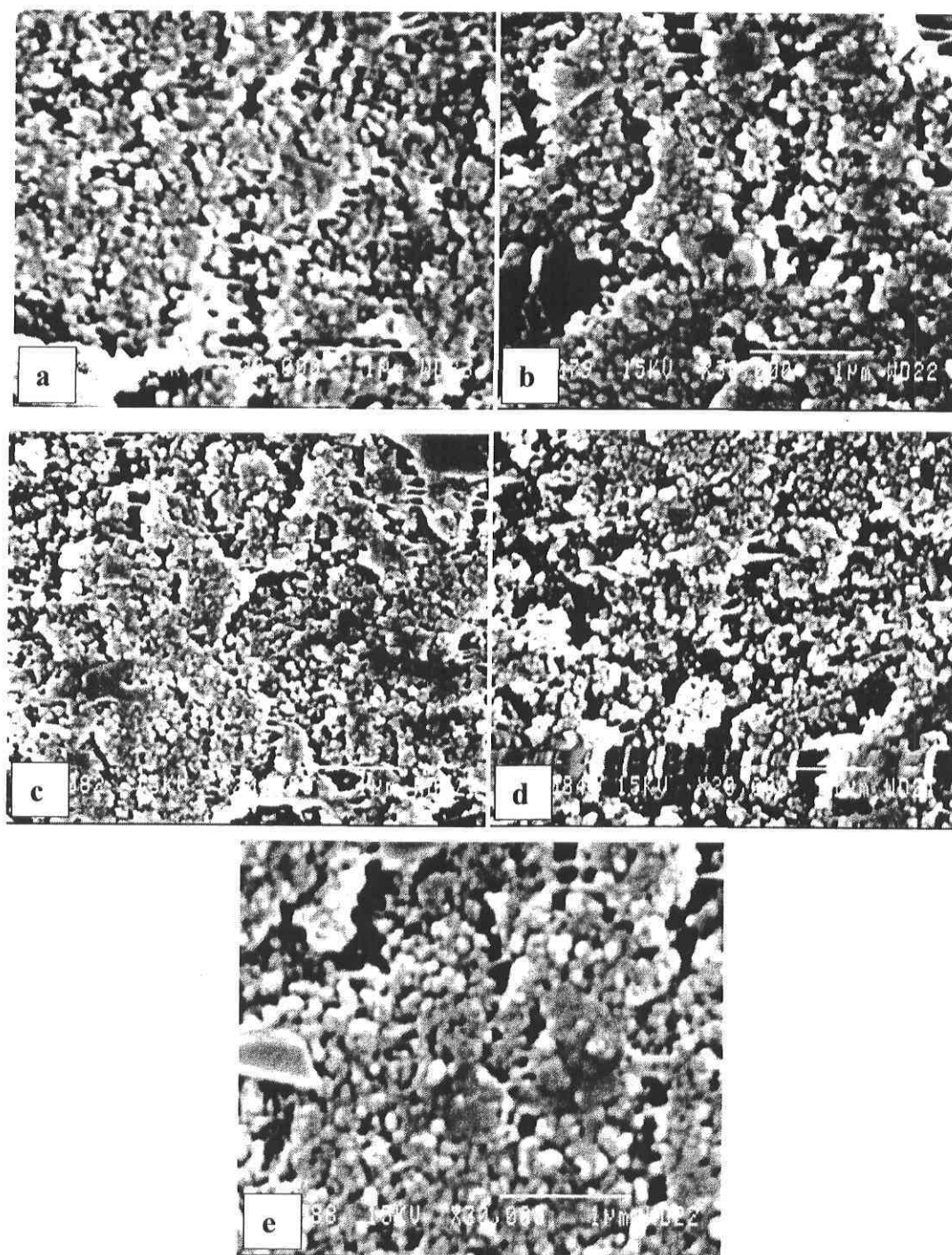
Figure 3-6 SEM micrographs of microporous films (uncompressed) after PS-1 extraction for different PS-1 phase concentrations. The films were microtomed along the extrusion direction; **a)** S-1, **b)** S-4, **c)** S-5, **d)** S-6, **e)** S-7.
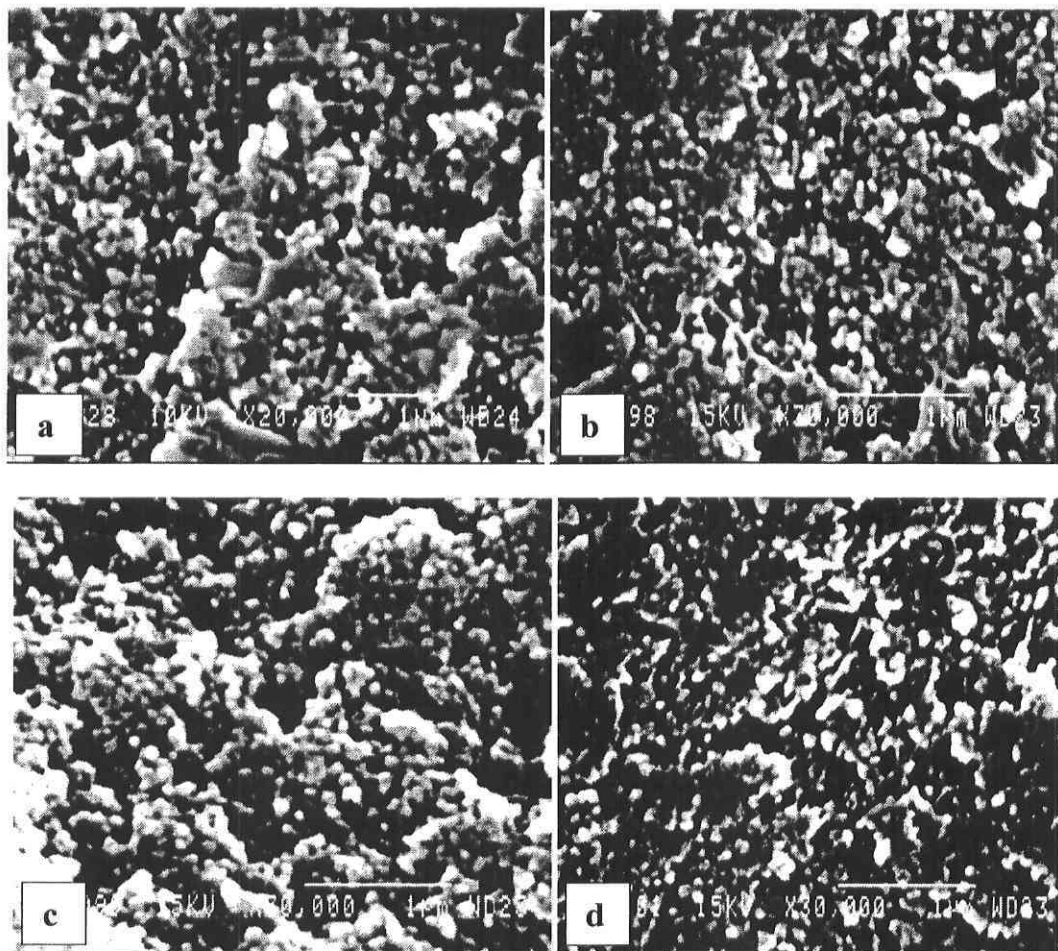
Figure 3-7 SEM micrographs of microporous films (uncompressed) after PS-1 extraction for different PS-1 phase concentrations. The films were microtomed perpendicular to the extrusion direction; **a)** S-4, **b)** S-5, **c)** S-6, **d)** S-7.

3.3.4 Film Porosity Characterization by BET and Mercury-Intrusion Techniques

3.3.4.1 BET Surface Area Characterization

Porosity characterization was done using the BET technique presented in Section 3.2.7.1. Figure 3-8 shows the linear relationship between $\dfrac{P}{V \cdot (P^o - P)}$ and $\dfrac{P}{P^o}$ obtained from Equation 3-3 for the seven developed films in which the weight fraction of PS-1 was varied from 25 to 42wt%. Form each film, the BET specific surface area (which is a measure of film porosity) was calculated using Equation 3-5 and the corresponding slope and intercept taken from Figure 3-8, as explained in Section 3.2.7.1.
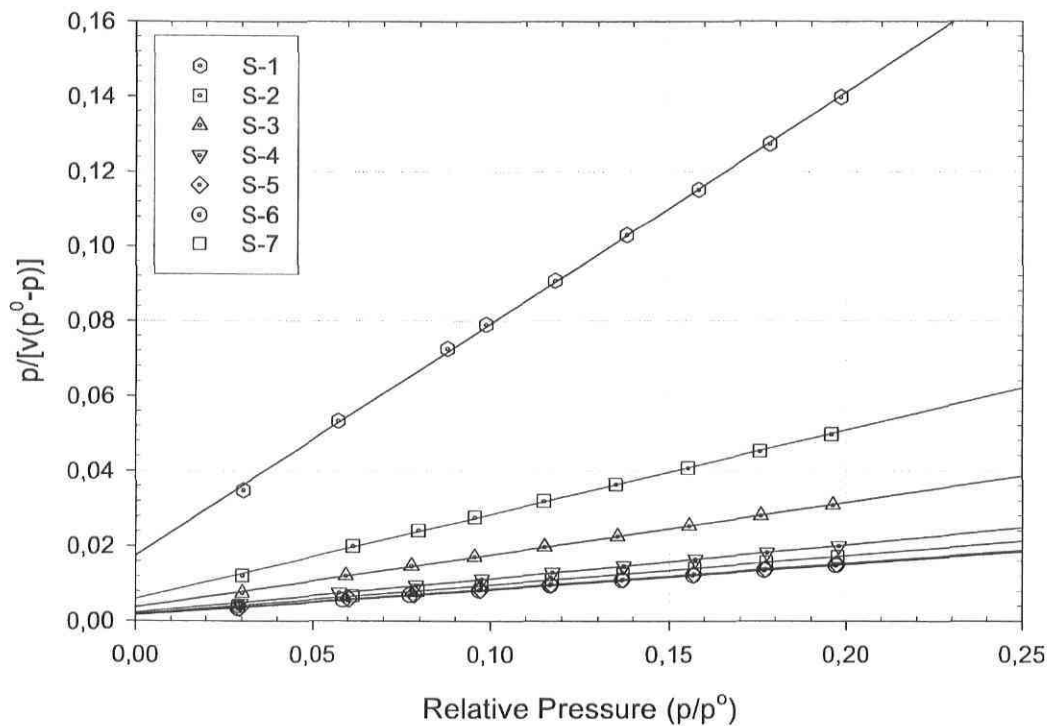

Figure 3-8 Relationship between $\dfrac{P}{V \cdot (P^o - P)}$ and $\dfrac{P}{P^o}$ obtained from Equation 3-3 for films made from blends S-1 to S-7 after PS-1 extraction by THF.
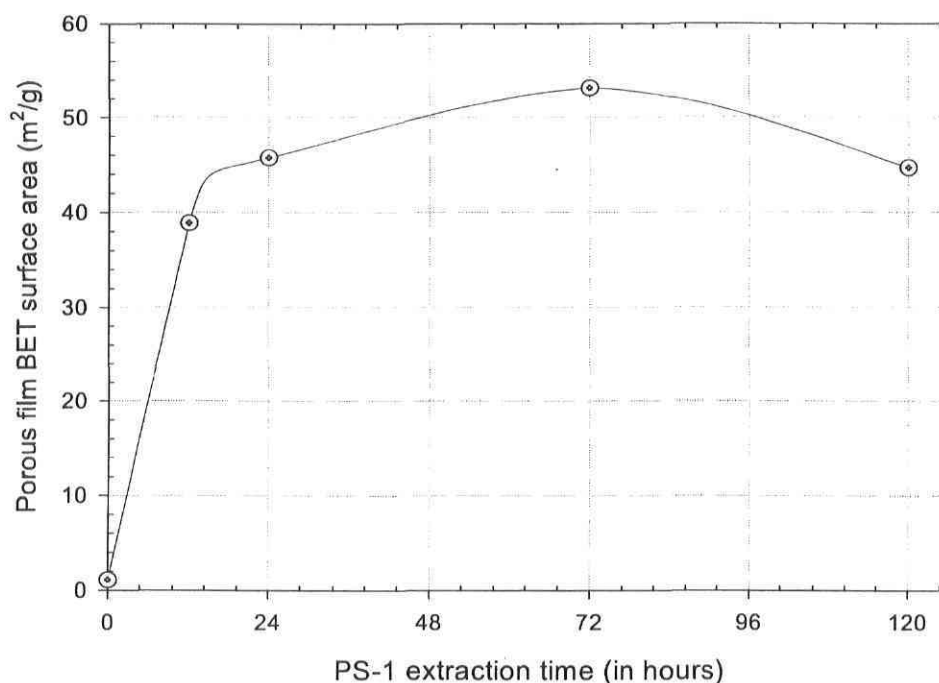
Figure 3-9 BET specific surface area and the corresponding pore average diameter for film made from blend S-4 as a function of PS-1 extraction time.

To elucidate the effect of PS-1 extracting time on specific pore surface area, one of the seven films studied, S-4, which has the following composition: 60wt% of (42/58 PP/PS) mixed with 40wt% of (60/40 CB/GR), was subjected to PS-1 extraction in THF solvent during 120 hours. Four BET measurements were then done at different extraction times (12, 24, 72 and 120 hours) and the corresponding results are presented in Figure 3-9, together with the corresponding pore average diameters. The BET surface area increases rapidly to around $40 \, m^2/g$ after the 12 first hours of PS-1 extraction then to around $54 \, m^2/g$ after 72 hours. For higher extraction time, the BET surface area decreases. This could be explained by the fact that, during the first period of extraction, the THF solvent didn't diffuse inside the whole PS-1 structure. With increasing time, THF continues to penetrate inside the PS-1 network to dissolve it and to generate more pores inside the film, resulting in an increase of the specific surface area. At a certain extraction time, many interconnected PS-1 particles are

completely extracted and transformed into large pores, due to void coalescence, leading to a decrease of the BET surface area. Based on the above results, the highest film porosity level was attained after around 72 hours.
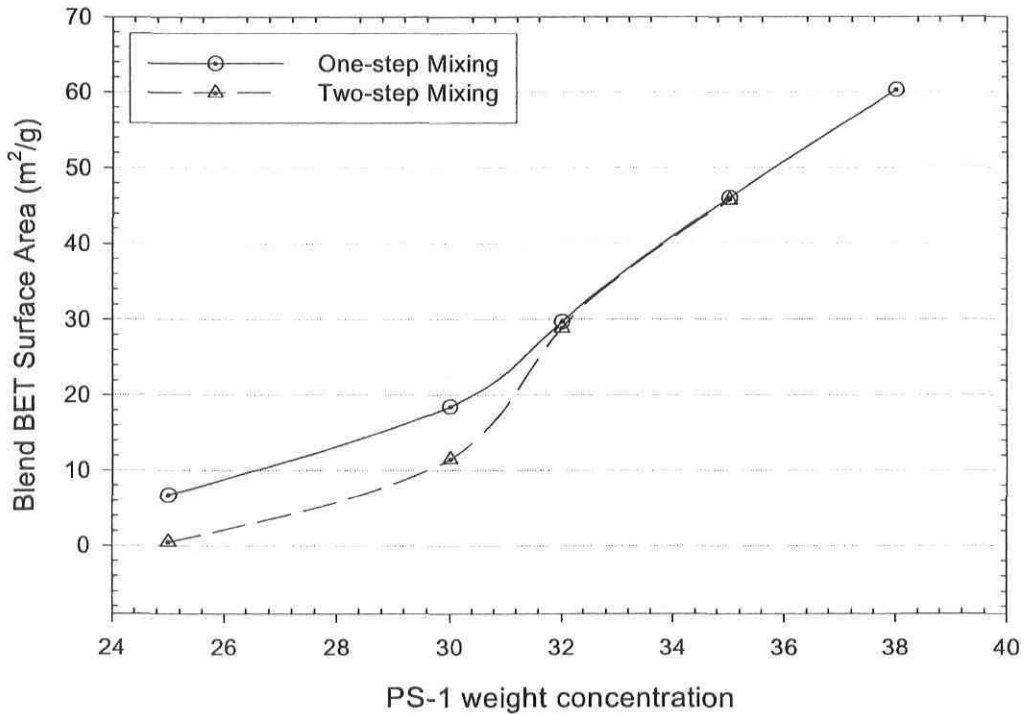
Figure 3-10 BET specific surface area as a function of PS-1 weight concentration for both one-step and two-steps mixing techniques.

Figure 3-10 shows the BET specific surface area, after 72 hours of PS-1 extraction in THF, for films made from blends S-1 to S-5 as a function of PS-1 weight concentration for both one-step and two-steps mixing techniques presented section 3.2.2. For PS-1 concentration less than 32wt%, the BET specific surface area for blends prepared via the two-steps mixing technique is lower than that obtained for blends prepared via the one-step mixing technique. However, for PS-1 higher concentrations, the two mixing techniques lead to the same BET surface areas.

Based on the resistivity, morphology and BET results, the two-steps mixing technique didn't show any evident improvement on both film resistivity and porosity, compared to the one-step mixing. The latter technique was then preferred due its lower processing time.
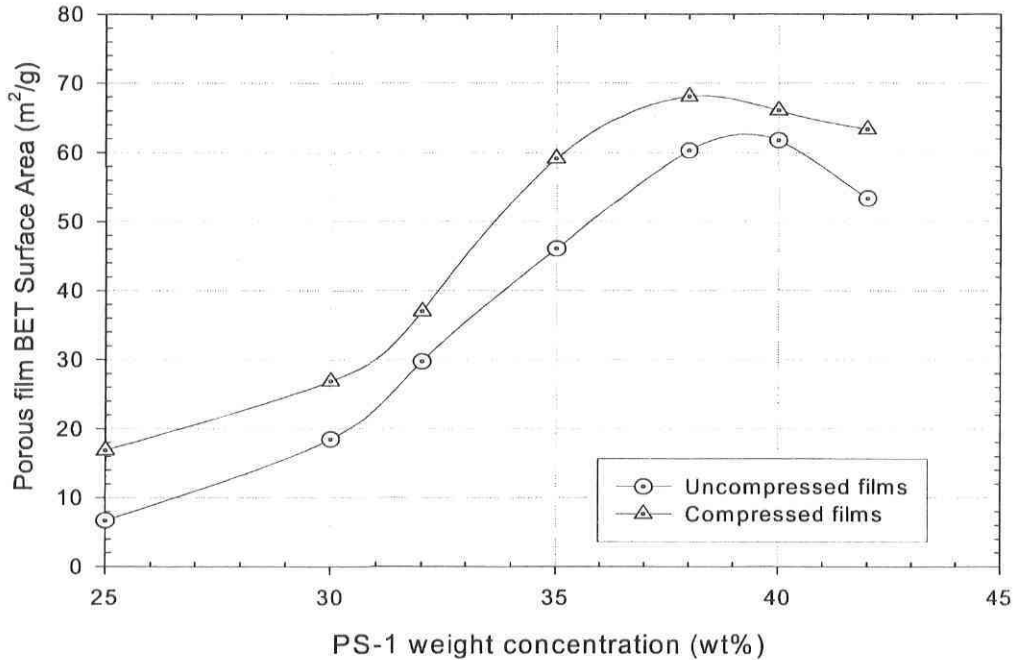
Figure 3-11 BET specific surface area of porous uncompressed and compressed films as a function of initial PS-1 concentration.

Figure 3-11 shows, for both uncompressed and compressed films made from blends S-1 to S-7, the evolution of BET surface area with PS-1 concentration after 72 hours of PS-1 extraction in THF solvent. Corresponding blends are always composed of 60wt% of PP/PS-1 polymeric phase and 40wt% of 60/40 CB/GR phase. For both compressed and uncompressed films, BET surface area increases with increasing PS-1 concentration up to around 38-40wt% and decreases for higher PS-1 concentration. From this result, it can be expected that the co-continuity of PP and PS-1 phase is reached between 38-40wt% of PS-1. To verify this, both resistivity and BET surface area of uncompressed films were replotted together, as a function of PS-1 weight concentration (Figure 3-12). Blend resistivity and BET surface area show

opposite behavior when the initial PS-1 weight fraction is increased. The resistivity decreases while the BET surface area increases when PS-1 concentration is increased up to 40wt%. However, above 40wt%, blend resistivity increases and surface area decreases. From this result, it can be concluded that 40wt% of PS-1 corresponds to the co-continuity concentration over which PS-1 pore dimensions start to decrease because of pore coalescence and the density of the conductive network built inside PP begin to decrease, leading to a decrease in conductivity (i.e., resistivity increases).
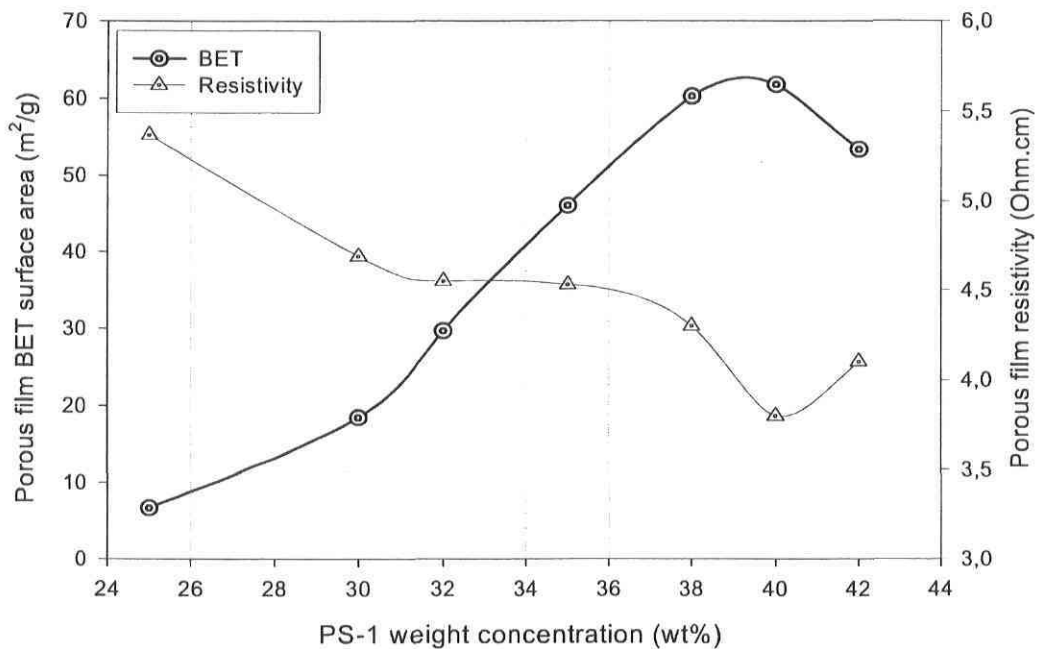

Figure 3-12 Resistivity and BET surface area of porous uncompressed films as a function of initial PS-1 concentration.

3.3.4.2 Pore Size Distribution

Some previous studies [12, 14, 24-27] have demonstrated the importance of GDL morphology, especially pore size distribution, on PEMFC performance. Presently, GDL are composed of carbon cloth or carbon paper that has macroporous structure on which carbon black powder and hydrophobic dispersion agent are applied by using an adequate solvent to form a second microporous layer. It should be mentioned that certain confusion exists in the literature concerning pore-size classification. Microporosity is generally used instead of mesoporosity. In the present study, the IUPAC (International Union of Pure and Applied Chemistry) criteria for classifying micropores (diameters less than 0.002 μm), mesopores (diameters between 0.002 and 0.05 μm), and macropores (diameters higher than 0.05 μm), was respected.

The specific and cumulative pore-size distributions for three compressed films made from blends S-5, S-6 and S-7 are shown in Figures 3-13(a) and (b), respectively. Figure 3-13(a) shows that the range of pore-size is distributed between 0.001 and 300 μm. Three main porous structures (micro, meso, and macroporous) coexist inside the films. However, as shown in Figure 3-13(b), the cumulative pore volume curve shows that mesopores occupy more than 60% of the total pore volume. The micro and mesoporosity correspond to those of CB and GR dispersed inside the PP matrix. However, the macroporous structure is created by the void spaces left by extracted PS-1 phase. Macropores are thought to reduce problems of mass-transport caused by water flooding and, hence, improve PEMFC performance [14].
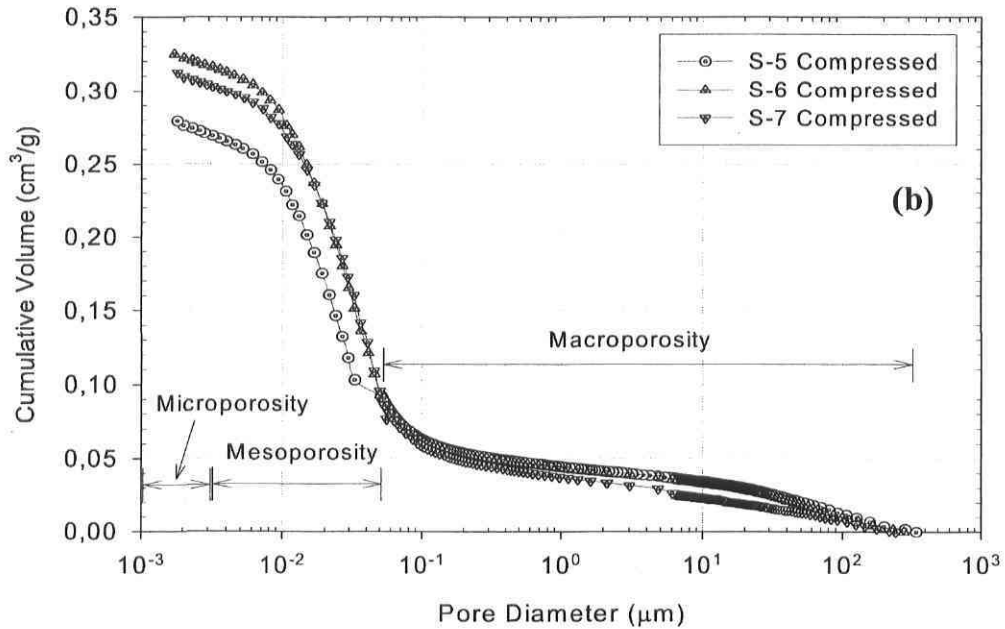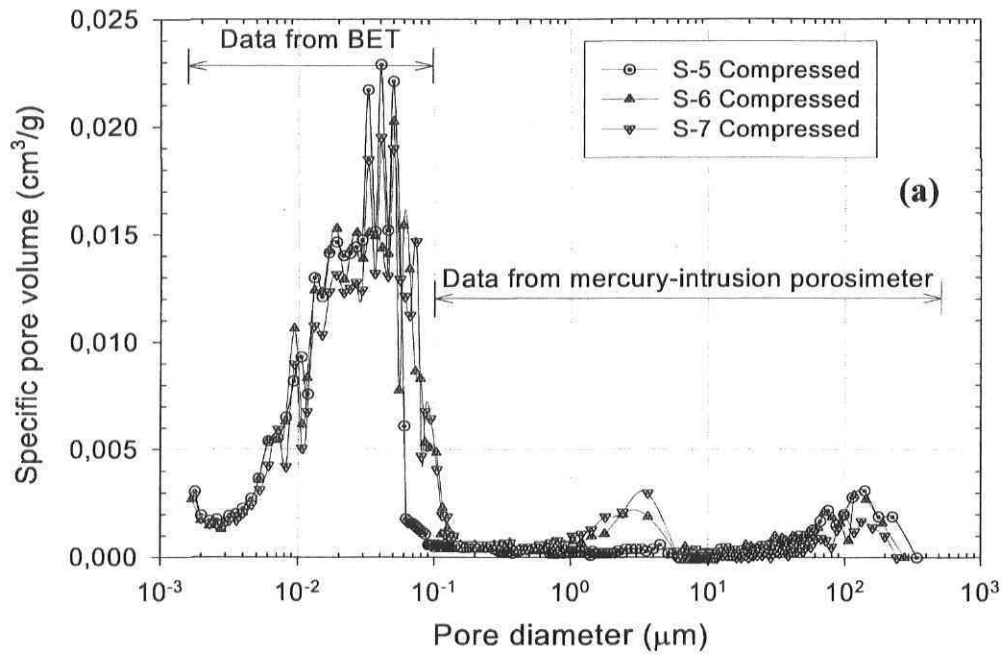
Figure 3-13 Pore-size distribution obtained by BET and mercury-intrusion techniques: **(a)** Specific pore volume, **(b)** Cumulative pore volume.

3.4 CONCLUSION

A microporous film structure for PEMFC electrode gas diffusion layer was developed from polypropylene/polystyrene mixture filled with electronic conductive carbon black and graphite additives. The conductive blends were first compounded then extruded in thin films using a co-rotating twin-screw extruder. The Polystyrene phase was then extracted from the extruded film with tetrahydrofuran solvent to generate the porosity needed for gas diffusion.

During the compounding/film extrusion step, thin films were successfully developed from optimized blends composed of 60wt% of Polypropylene/Polystyrene phase and 40wt% of 60/40 Carbon black/graphite additives. Film in-plane and through plane resistivities of around 0.55 and 3.8 Ohm-cm, respectively, were achieved. The in-plane resistivity (i.e., along the extrusion direction) is lower than that perpendicular to flow direction due to conductive filler orientation along flow direction.

Film conductivity and porosity were optimized; first, by selecting the initial concentrations of PP/PS and CB/GR phases, then by adjusting the composition of the PP/PS polymeric phase. Optimized porosity and conductivity were achieved for PS weight concentration situated between 38 and 40wt%.

LIST OF SYMBOL

ρ	Resistivity $(\Omega.cm)$.
R	Resistance (Ω).
t	Film thickness (cm).
w	Width of samples (cm).
l	Distance between two probes (cm).
D	Electrode diameter (cm).
P	Vapor pressure of the gas (mmHg).
P^o	Equilibrium vapor pressure of the gas (mmHg).
V	Volume of absorbed gas at experimental pressure (cm^3/g).
V_m	Volume of adsorbed gas at STP (cm^3/g).
c	Constant related to the energy of adsorption.
E_1	Heat adsorption for the first layer (J/mol).
E_L	Heat adsorption for the second and higher layer (J/mol).
R	Universal gas constant ($J.mol^{-1}.K^{-1}$).
T	Temperature (K).
S	Specific surface area (m^2/g).
N	Avogadro's number (molecule/mol).
a	The area corresponding to one adsorbed nitrogen molecules (m^2/molecule).
υ_m	Molar volume of the gas at STP (L/mol).

REFERENCES

[1]   P. Costamagna, S. Srinivasan, J. Power Sources, 102 (2001) 242.

[2]   G. Hoogers, "Fuel cell Technology Handbook", CRC press, New York, 2003, p1.

[3]   G. Alberti and M. Casciola, Solid State Ionics, 145 (2001), 3.

[4]   E. A. Ticianelli, C. R. Derouin, A. Redondo, S. Srinivasan, J. Electrochem. Soc., 135 (1988), 2209.

[5]   S. J. Lee, S. Mukerjee, J. McBreen, Y. W. Rho, Y. T. Kho, T. H. Lee, Electrochim. Acta, 43 (1998), 3693.

[6]   X. Cheng, B. Yi, M. Han, J. Zhang, Y. Qiao, J. Yu, J. Power Sources, 79 (1999), 75.

[7]   Y. G. Chun, C. S. Kim, D. H. Peck, D. R. Shin, J. Power Sources, 71 (1998), 174.

[8]   Z. Qi, A. Kaufman, J. Power Sources, 113 (2003), 37.

[9]   S. Litster, G. McLean, J. Power Sources, 130 (2004), 61.

[10]   S. Hirano, J. Kim, S. Srinivasan, Electrochim. Acta, 42 (1997), 1587.

[11]   S. Swathirajan and Y. M. Mikhail, The Electrochemical Society Proceedings Series, Pennington, NJ, 1994, 158.

[12]   L. Giorgi, E.Antoloni, A. Pozio and E. Passalacqua, Electrochim. Acta, 43 (1998), 3675.

[13]   M. Glora, M. Wiener, R. Petricevic, H. Probstle, J. Fricke, Journal of Non-Crytalline Solids, 285 (2001), 283.

[14]   C. S. Kong, D. Y. Kim, H. K. Lee, Y. G. Shul, T-H.Lee, J. Power Sources, 108 (2002), 185.

[15]   E. Antolini, R. R. Passos, E. A. Ticianelli, J. Power Sources, 109 (2002), 477.

[16] J. M. Song, S. Y. Cha, W. M. Lee, J. Power Sources, 94 (2001), 78.

[17] Z. Qi, A. Kaufman, J. Power Sources, 109 (2002), 38.

[18] F. Mighri, M. A. Huneault, M. F. Champagne, Polym. Eng. Sci., 44 (2004), 1755.

[19] M. H. Oh, Y. S. Yoon, S. G. Park, Electrochim. Acta, 50 (2004), 777.

[20] A. Hermann, T. Chaudhuri, P. Spagnol, Int. J. Hydrogen Energy, 30 (2005), 1297.

[21] M. C. Collier and D. G. Baird, Polymer Composites, 20 (1999), 423.

[22] S. Brunauer, P. H. Emmett, E. Teller, Journal of American Chemical Society, 60 (1938), 309.

[23] US Patent, 5863673 (1999), S. A. Campbell, J. Stumper, D. P. Wilkinson, M. T. Davis.

[24] D. M. Bernardi and M. W. Vebrugge, J. Electrochem. Soc., 139 (1992), 2477.

[25] M. S. Wilson, J. A. Valerio, S. Gottesfeld, Electrochim. Acta, 40 (1995), 355.

[26] H.L. Lee, J.H. Park, D.Y Kim, T.H. Lee, J. Power Sources, 131 (2004), 200.

[27] E. Passalacqua, G. Squadrito, F. Lufrano, A. Patti, L.Giorgi, J.Appl. Electrochem., 31 (2001), 449.

CHAPTER 4

Conclusions and Recommendations

This thesis concerns the development of porous conductive films for PEMFC electrode gas diffusion layers. During this study, helpful information about the formulation of conductive blends by using co-rotating twin-screw extruder and about techniques to generate film porous structures has been acquired. The effect of conductive additives concentration on extruded film resistivity and processability was investigated. Blend resistivity and processability were related to the conductive additives structure and the processing methods.

In the first part of the thesis, a critical literature review was presented about the PEMFC and the present techniques used for their manufacturing. A special attention was given to PEMFC electrodes and electrode gas diffusion layer, especially to their conventional production methods. The main objectives of this thesis were presented together with the adopted new processing techniques.

Two different techniques were used to generate the porosity inside the conductive extruded films. For each technique, the effect of processing conditions on film porosity was studied separately.

The first technique to generate films with porous structure is presented in chapter 2. Conductive blends based on PP, CB and GR were first prepared using a co-rotating twin screw extruder then extruded through a thin sheet die to obtain non-porous conductive films. During

a post-extrusion step, these films were uniaxially stretched in order to generate the needed porosity. To the best of our knowledge, this technique was used for the first time on films made from highly filled polymers. Big efforts were spent for process optimization for both extrusion and stretching steps. However, further morphological study is still required to obtain more accurate information about the porous structure. Because the extruder used in this study was not equipped with a calendaring system to control film thickness and thickness uniformity, a post-extrusion compression was done on extruded films. Compression effect on film conductivity was evaluated for different conductive additive concentration. It was found that film compression increases its conductivity.

Chapter 3 presents the results obtained with a second processing technique, which consisted in film extrusion followed by selective dissolution treatment. A porous film structure was developed from polypropylene/polystyrene mixture filled with electronic conductive carbon black and graphite additives. The Polystyrene phase was then extracted from the extruded film with tetrahydrofuran solvent to generate the porosity needed for gas diffusion and water management inside the PEMFC electrode. Thin films were successfully developed from optimized blends composed of 60wt% of Polypropylene/Polystyrene phase and 40wt% of 60/40 Carbon black/graphite additives. Film in-plane and through plane resistivities of around 0.55 and 3.8 Ohm-cm were respectively achieved. Film conductivity and porosity were optimized; first, by selecting the initial concentrations of PP/PS and CB/GR phases, then by adjusting the composition of the PP/PS polymeric phase. Optimized porosity and conductivity were achieved for PS weight concentration situated between 38 and 40wt%. The polystyrene extraction time and its effect on film porosity were also studied. It was found that, for short extraction times, THF solvent was not able to penetrate inside all polystyrene networks and to dissolve it. Ideal extraction time was found to be equal to 72 hours at room temperature.

It is worth noting that the two techniques used during this study to develop the porous films for PEMFC gas diffusion layers have several advantages compared to the conventional fabrication methods presently used. By adopting the two proposed techniques detailed in this thesis, film structure can be tailored by adjusting blend components and/or processing parameters.

In the present work, high electrical conductivity was ensured by using two kinds of carbon based materials: carbon black and graphite. The main reason for the difficulties encountered during film extrusion was the blockage of the die due to the high viscosity of the filled polymers. It is recommended in a future study to investigate other conductive additives that can ensure high conductivity at low concentration. For this purpose, other kinds of carbon based materials should be analyzed. Carbon nanotubes could be explored as an alternative to the carbon black and graphite. However, this highly conductive material remains expensive for industrial use. In order to improve the stretching process used in the first technique, a more adequate system is required for the stretching post-extrusion step. Biaxial stretching treatments could lead to better porosity results.

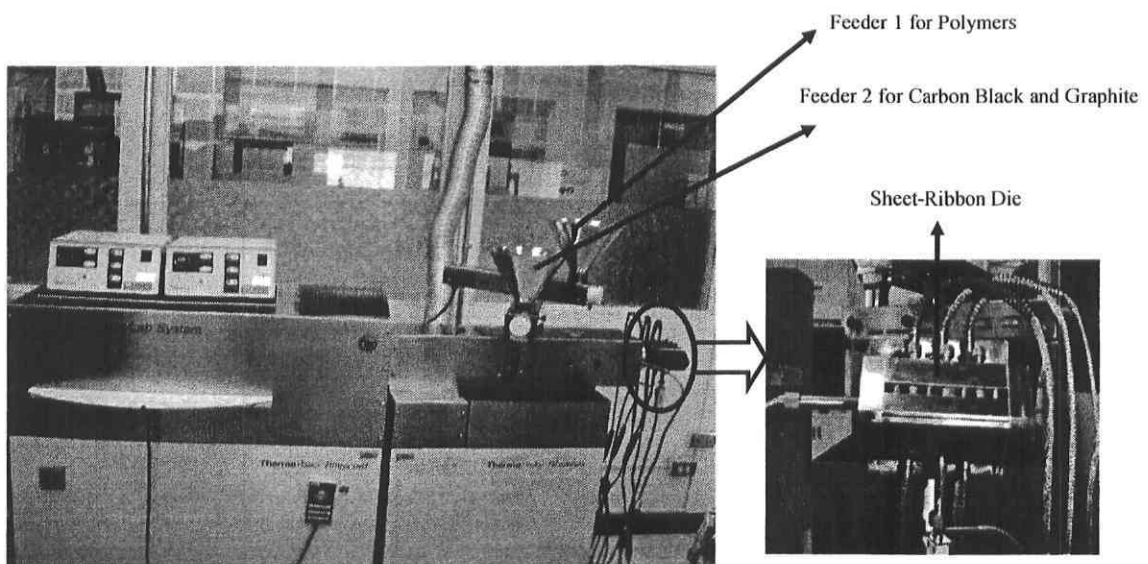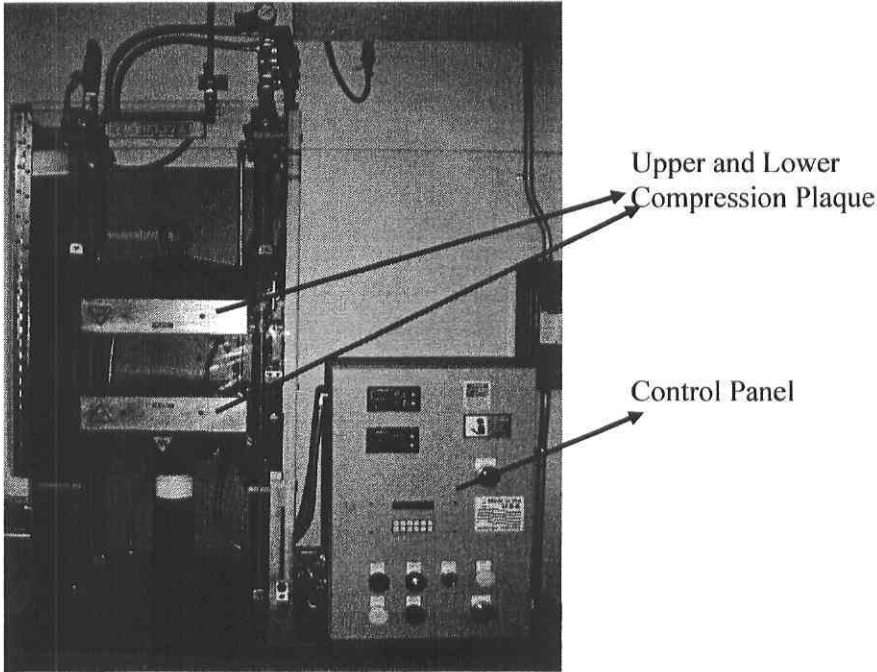## Experimental Devices

---

A) Co-Rotating Twin Screw Extruder

Feeder 1 for Polymers

Feeder 2 for Carbon Black and Graphite

Sheet-Ribbon Die

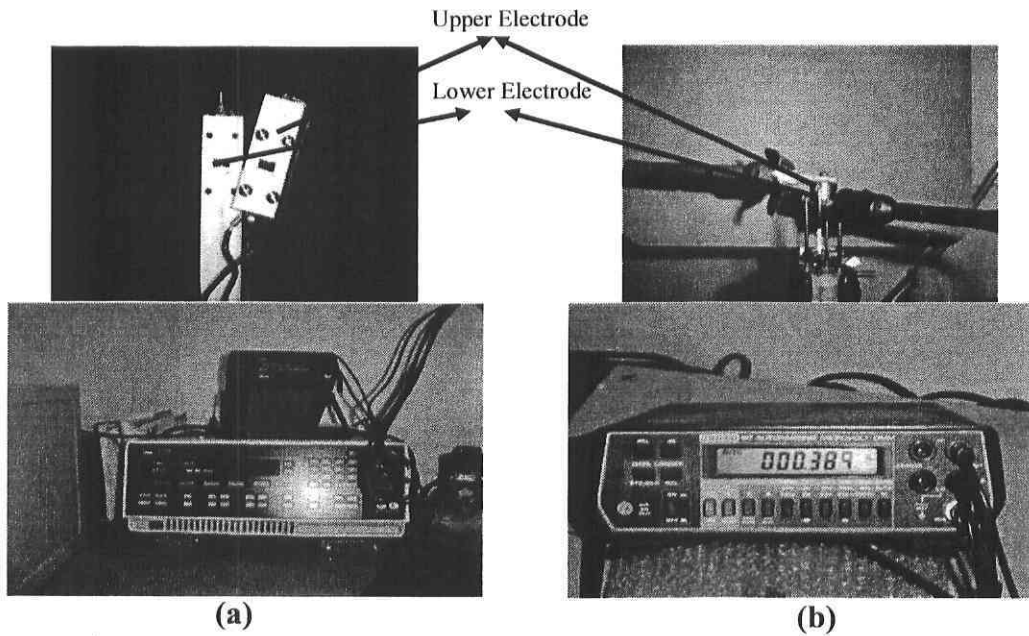**Figure A-1** ThermoHaake Polylab System, Rheomex.

B) Compression Machine

Upper and Lower Compression Plaque

Control Panel

Figure A-2 Carver Compression Machine.

C) Axial Stretcher

Heat Chamber

Upper and Lower Grips

Sample
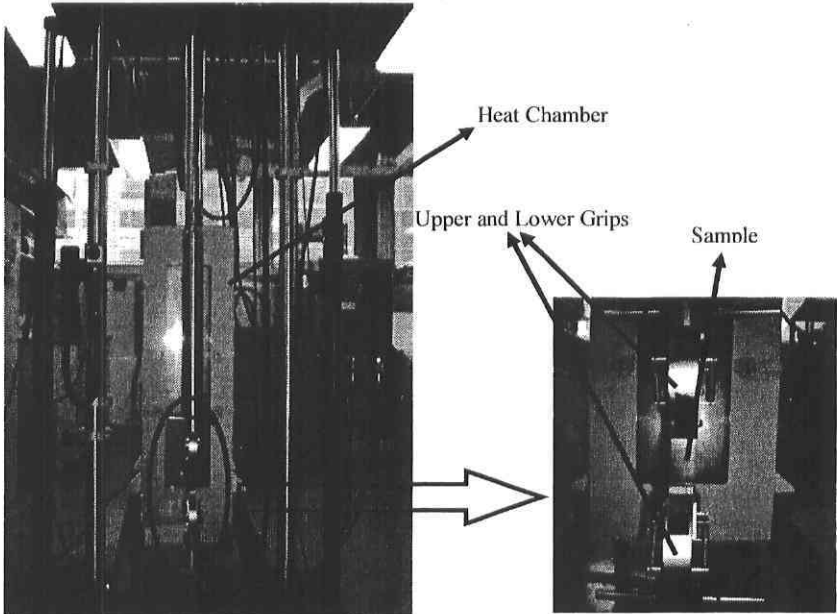
Figure A-3 Instron 8821S.

D) Instruments for Resistivity Characterization

Figure A-4 (a) Solartron SI1260 and an electrode for measuring in-plane resistivity, (b) Keithley Model 197 and an electrode for measuring through-plane resistivity.
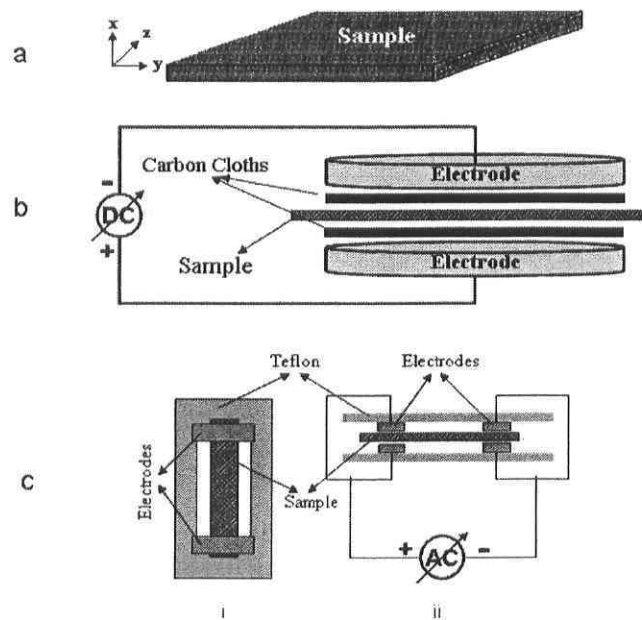
Figure A-5 Electrical resistivity measurement setup, a) representation of a sample, b) electrode connection for through plane resistivity, c) electrode connection for in-plane resisitivity, i) top view of electrode, ii) side view of electrode.

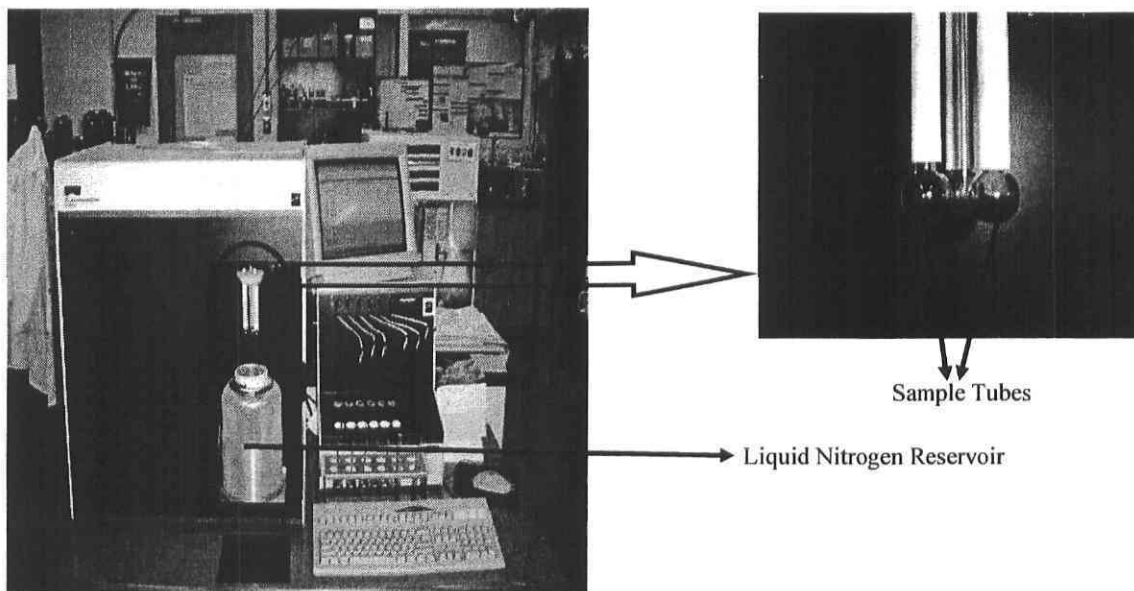## E) Instruments for Porosity Characterization

Sample Tubes

Liquid Nitrogen Reservoir

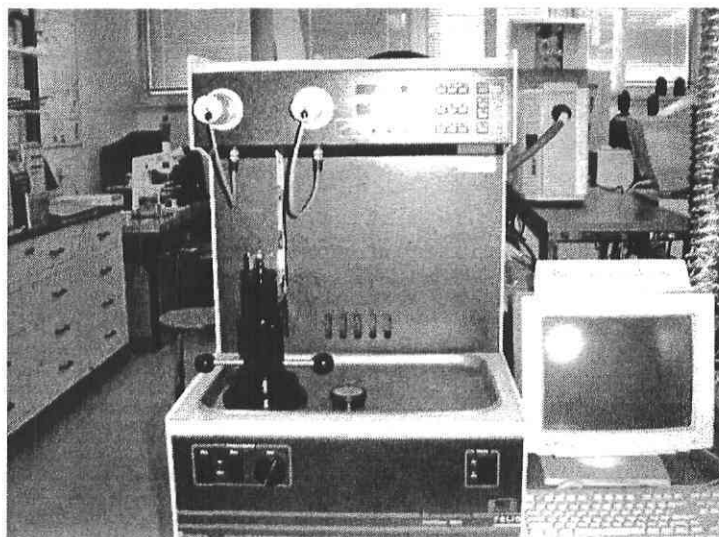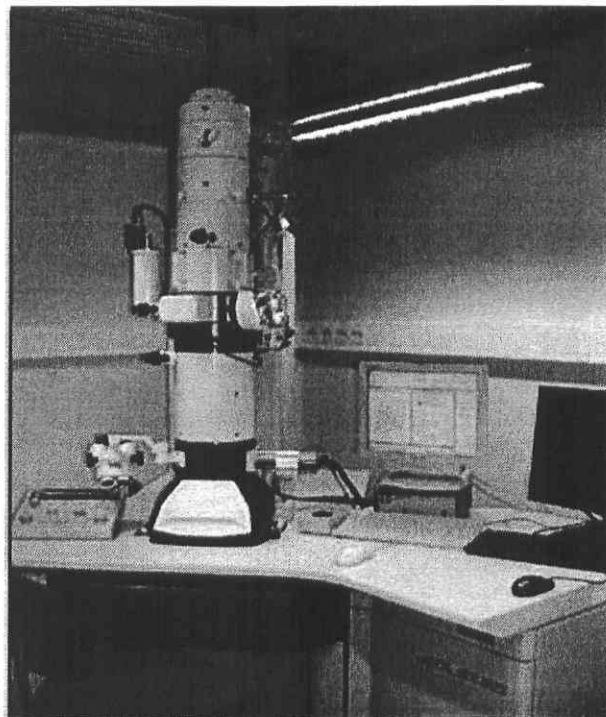**Figure A-5** BET, Tristar-3000, Micromeritics.

Figure A-6 Mercury Porosimetry, Porosizer 9320, Micromeritics.

F) Instruments for Morphology Characterization

Figure A-7 Scanning Electron Microscopy, JSM 840A, Jeol.

Figure A-8 Transmission Electron Microscopy, JEM-1230, Jeol.